nature biotechnology

Article

https://doi.org/10.1038/s41587-024-02271-7

Programming tumor evolution with selection gene drives to proactively combat drug resistance

Received: 30 May 2023

Accepted: 6 May 2024

Published online: 04 July 2024

Check for updates

Scott M. Leighow[1,2], Joshua A. Reynolds[1], Ivan Sokirniy[1,2], Shun Yao[2,3], Zeyu Yang[1], Haider Inam[1], Dominik Wodarz[4], Marco Archetti[2,3] & Justin R. Pritchard[1,2]

Most targeted anticancer therapies fail due to drug resistance evolution. Here we show that tumor evolution can be reproducibly redirected to engineer therapeutic opportunity, regardless of the exact ensemble of pre-existing genetic heterogeneity. We develop a selection gene drive system that is stably introduced into cancer cells and is composed of two genes, or switches, that couple an inducible fitness advantage with a shared fitness cost. Using stochastic models of evolutionary dynamics, we identify the design criteria for selection gene drives. We then build prototypes that harness the selective pressure of multiple approved tyrosine kinase inhibitors and employ therapeutic mechanisms as diverse as prodrug catalysis and immune activity induction. We show that selection gene drives can eradicate diverse forms of genetic resistance in vitro. Finally, we demonstrate that model-informed switch engagement effectively targets pre-existing resistance in mouse models of solid tumors. These results establish selection gene drives as a powerful framework for evolution-guided anticancer therapy.

For many cancers, drug resistance evolution represents one of the greatest challenges to the development of curative anticancer therapies. Studies of single-cell heterogeneity have revealed that small resistant subclones often exist in the tumor at baseline[1,2], suggesting that most cases will result in treatment failure. Moreover, recent studies in hundreds of patients with advanced lung cancer have unearthed a startling level of underlying genetic diversity within and across patients but reveal few clues on how to combat this profound heterogeneity[3,4]. Drug treatment dramatically reshapes the evolutionary landscape of the tumor, and the result is often selection for a drug-refractory tumor with fewer available treatment options.

Efforts to combat resistance are hindered by the intrinsic uncertainty of resistance evolution. In most cases, resistance variants are too rare to reliably detect at the beginning of treatment[5,6], and so the evolutionary trajectory of the tumor cannot be predicted. Thus, the conventional approach to treating resistance involves waiting for subclones to grow large enough to be clinically detectable, and then responding with an appropriate therapeutic strategy[7]. In the case of targeted therapy, where resistance can be driven by point mutations in the target gene, this strategy often means developing and responding with next-generation inhibitors. For example, in *EGFR*-mutant non-small-cell lung cancer (NSCLC), the next-generation tyrosine kinase inhibitor (TKI) osimertinib is indicated for tumors treated in the frontline with the TKI erlotinib that have acquired a T790M resistance mutation. However, these next-generation therapies generally offer only temporary responses[8]. The practice of waiting for resistance outgrowth during frontline therapy provides sufficient time and selective pressure to allow for the emergence of secondary resistance (Fig. 1a). In the

[1]Department of Biomedical Engineering, The Pennsylvania State University, University Park, PA, USA. [2]Huck Institute For The Life Sciences, The Pennsylvania State University, University Park, PA, USA. [3]Department of Biology, The Pennsylvania State University, University Park, PA, USA. [4]Department of Biology, University of California San Diego, San Diego, CA, USA. e-mail: jrp94@psu.edu

case of *EGFR*-mutant NSCLC, erlotinib-refractory tumors treated with osimertinib often acquire the secondary resistance mutation C797S.

At the scale of the pharmaceutical industry, tremendous resources are invested in next-generation drug development in an attempt to stay ahead in this evolutionary arms race. At the scale of the individual patient, sequential monotherapy allows the tumor to evade each iteration of treatment until all available therapeutic options are exhausted.

Theoretical[9,10] and empirical evidence[11,12] suggests that the only way to outpace resistance evolution is to employ combination therapies at the beginning of treatment. By combining agents with distinct mechanisms of resistance, the risk of cross-resistance is minimized. However, the development of rational therapies that inhibit independent oncogenic programs is fundamentally limited by our ability to identify orthogonal targets. An ideal novel target with a unique mechanism of action should have completely distinct resistance mechanisms and nonoverlapping dose-limiting toxicities. For example, in *EGFR*-mutant NSCLC, efficacious combination therapy would require the identification of a genetic vulnerability that is as essential as *EGFR* but when drugged produces a completely orthogonal set of resistance mutations outside of existing RTK/MAPK resistance pathways and distinct dose-limiting toxicities. However, large-scale mapping of genetic dependencies has underscored the paucity of these selectively essential targets beyond growth receptor signaling pathways[13,14], suggesting there is a limited potential to develop targeted combination therapies with truly orthogonal modes of action.

Moreover, the US Food and Drug Administration has recently approved osimertinib with more broadly cytotoxic systemic chemotherapies[15], but the marginal benefit of these combinations is limited by the small therapeutic window of cytotoxic agents[16,17]. As a result, a majority of patients treated with EGFR inhibitor +chemotherapy combinations experience high-grade adverse effects, and long-term survival rates remain low[18,19]. Finally, *EGFR*-mutant tumors are neoantigen poor and thought to be unsuitable candidates for combinations of targeted therapies and immunotherapies[20,21]. These challenges hinder the development of treatment strategies that might have curative potential among advanced cancers treated with targeted therapies.

Rather than search for new drug targets, alternative treatment strategies have sought to genetically modify cancer cells to artificially introduce exogenous, therapeutically actionable genes. Gene-directed enzyme prodrug therapy (GDEPT) involves introducing a 'suicide gene' into cancer cells to locally activate an inert prodrug[22–24]. The activated metabolite is generally diffusible, enabling GDEPT to target both modified and nearby, unmodified cancer cells. However, clinical evaluations of suicide gene therapy have yielded underwhelming results[24–26]. This is often because poor gene delivery is a major challenge in GDEPT that precludes the potential for eradication, even with the noted bystander activity[27].

Introducing exogenous drug targets is challenging, and sequential monotherapy ensures that clinical efforts always remain one step behind cancer. The iterative approach of serial single-agent therapy resembles 'reverse engineering' resistance evolution: after treatment failure has occurred, the nature of resistance is characterized, and an appropriate treatment response is tailored to it (Fig. 1a). Here, we propose an alternative treatment strategy that 'forward engineers' evolution to redesign tumors so that they are more responsive to therapeutic intervention (Fig. 1b). This approach involves genetically modifying cancer cells in situ, and then using small molecules to invert the tumor's evolutionary landscape to select for modified cancer cells in favor of resistant subclones. In re-engineering the tumor, we can exploit drug selection to generate more therapeutic opportunity, not less.

Inspired by clustered regularly interspaced short palindromic repeats (CRISPR)-based systems to control disease vector evolution[28], we term this approach 'dual-switch selection gene drives'. The genetic circuit is composed of two genes, or 'switches', that are stably introduced into cancer cells with a single vector. The fundamental function of this modular platform is to couple an inducible fitness advantage (Switch 1) with a shared fitness cost (Switch 2; Fig. 1c). Switch 1 acts as a synthetic resistance gene, endowing a transient resistance phenotype that amplifies the frequency of the engineered cells during treatment (Fig. 1d). Switch 2 is a therapeutic payload gene. As in standard GDEPT, it activates a diffusible therapeutic that kills both engineered and unmodified cancer cells. This bystander effect is amplified by hitchhiking on the Switch 1 gene, thus maximizing the therapeutic potential of the suicide gene. This bystander activity is agnostic to whatever native resistant populations are selected for during the Switch 1 phase of treatment. Additionally, because Switch 2 activity is, in theory, limited to the tumor environment, a higher local concentration of the activated agent might be safely achieved than would be possible through systemic administration[29]. By facilitating more potent therapeutic action, the risk of cross-resistance is minimized and the promises of combination therapy may be fully realized.

In this Article, we use model-informed designs to construct and evaluate dual-switch selection gene drives for anticancer therapy. By engineering inducible drug target analogs, we demonstrate controllable Switch 1 activity in multiple biological contexts. Moreover, we establish therapeutic function and bystander killing for GDEPT and immune versions of the Switch 2 gene. Our complete dual-switch circuits demonstrate the ability to eliminate pre-existing resistance, including complex genetic libraries of resistance variants within a drug target and across the genome. Finally, model-guided switch engagement demonstrates robust efficacy in vivo, highlighting the benefits of leveraging evolutionary principles rather than combating them. In total, our findings support the conceptual framework that selection gene drives rooted in evolutionary theory can be used to re-engineer tumors and target diverse forms of native genetic heterogeneity.

Results

Theory outlines design criteria for selection gene drives

Introducing and selecting for this genetic construct involves introducing more heterogeneity into a tumor population and intentionally

Fig. 1 | Compartmental and agent-based stochastic models of disease evolution establish criteria for gene drive design. a, Schematic of population dynamics for a tumor undergoing sequential monotherapy. **b**, Schematic of population dynamics for a 'forward engineering' approach to cancer therapy. An engineered population is selected for during the Switch 1 phase of treatment. Then, a suicide gene with a bystander effect is used to eliminate engineered and resistant cells during the Switch 2 phase of treatment. **c**, Schematic of modular dual-switch gene drive design. Both genetic switches are integrated into a single genetic circuit. **d**, Schematics for Switch 1 and Switch 2 activity. Under Switch 1 (left), targeted therapy is effective against sensitive cells (blue), but not resistant cells (red). Additionally, engineered gene drive cells (green) are rescued from therapeutic killing by Switch 1 function. Under Switch 2 (right), gene drive cells activate a prodrug with diffusible activity. The activated metabolite targets gene drive cells and neighboring unmodified cells via a bystander effect. **e**, Map of mutational pathways (that is, points of potential system failure) included in the compartmental dynamic model. **f**, Trajectory for one simulation of the compartmental model. Tumor detection size $M = 10^9$ cells; mutation rate $\mu = 10^{-8}$; infection efficiency $q = 5\%$; net growth rate of gene drive cells $\gamma_{gd} = 0.01$ (equal fitness to resistant cells). **g**, Summary of parameter sweep for compartmental model. Initial gene drive frequency (q) and net growth rate of gene drive cells (γ_{gd}) are allowed to vary. Net growth rate is shown as proportion relative to native resistant populations. Each parameter set is the frequency of eradication for 48 independent simulations. **h**, Example initial condition for spatial agent-based model with low dispersion. **i**, Example initial condition for spatial agent-based model with high dispersion. **j**, Summary of parameter sweep for spatial agent-based model. Bystander distance (that is, kill radius, ρ) and dispersion parameter ($1/\theta$) are allowed to vary. Dispersion is represented as the proportion of the theoretical maximum inter-cell gene drive distance. Each parameter set is the frequency of eradication for 25 independent simulations.

https://doi.org/10.1038/s41587-024-02271-7

expanding the genetically modified cancer cell population. To assess the mutational risks of this counterintuitive therapeutic approach, we developed a stochastic mechanistic model of tumor evolution. Such a model enables the anticipation and investigation of evolutionary risks associated with a selection gene drive system. Additionally, an understanding of the expected evolutionary dynamics under selection

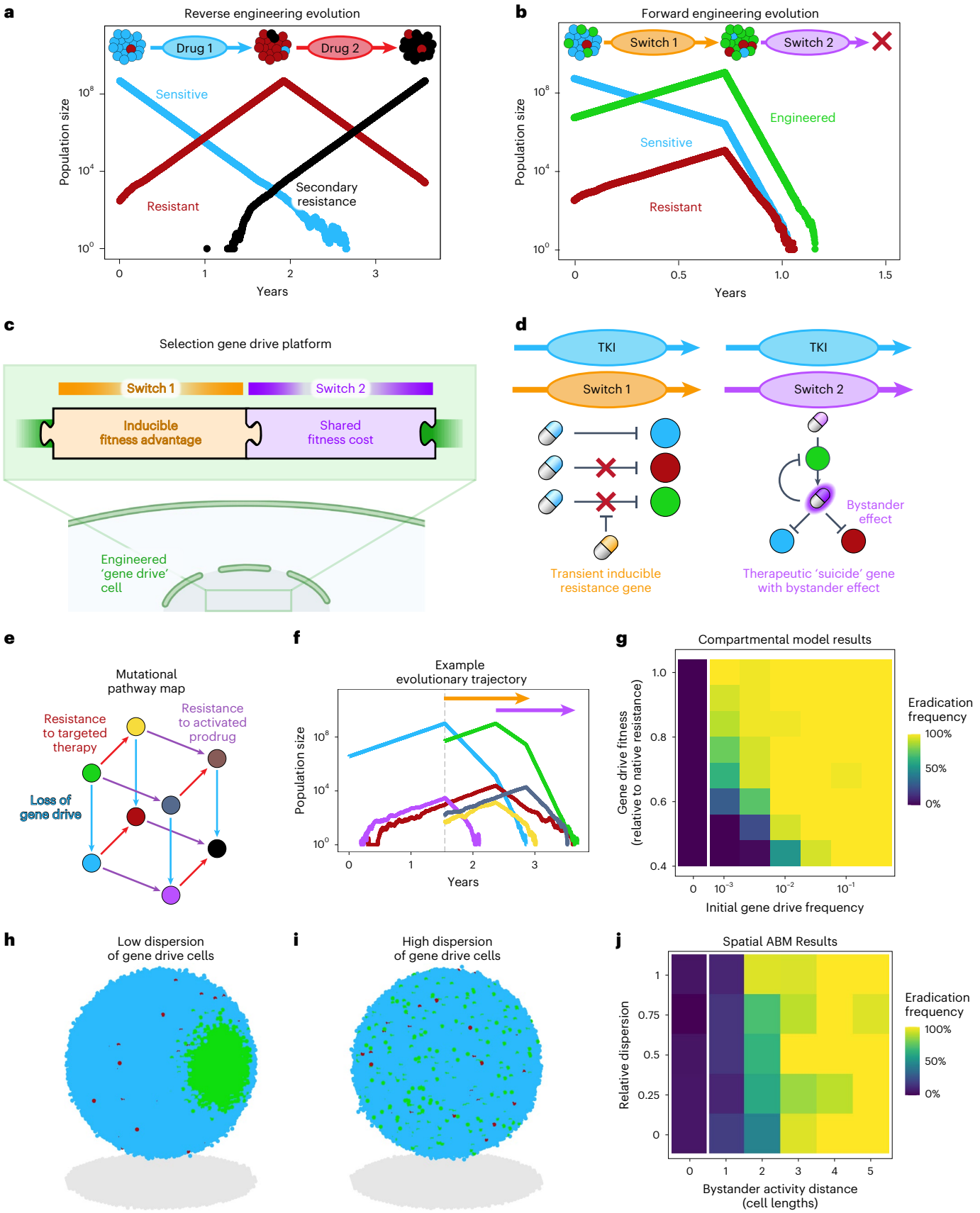

https://doi.org/10.1038/s41587-024-02271-7

gene drive therapy can inform key design criteria. These criteria span important aspects of the system, including the hypothetical gene delivery efficiency required to achieve evolutionary control and the fitness of gene drive cells in the Switch 1 treatment phase necessary to outcompete native resistance.

The model considers a small, initially sensitive population of cancer cells that expand until, upon tumor detection, a fraction of tumor cells is modified to become gene drive cells and treatment is initiated. The Switch 1 phase of treatment is maintained until gene drive cells become the dominant population, whereupon Switch 2 treatment begins. Over the course of the simulation, mutation events spawn subclones that model potential points of system failure. These mutations include acquired resistance to targeted therapy, resistance to the therapeutic action of the Switch 2 gene and loss of Switch 2 activity among gene drive cells (Fig. 1e). The compartmental model assumes that no single mutation confers resistance to both forms of therapy and homogeneous drug exposure.

We simulated this system for a large range of model parameters. The evolutionary trajectory for one such simulation is shown in Fig. 1f. Analysis of simulation results indicates that gene delivery need not be very efficient. The model demonstrates that selection under Switch 1 can overcome limitations imposed by poor gene uptake, and evolutionary control is predicted to be possible for <1% initial gene drive population under some conditions (Fig. 1g). Additionally, simulation results suggest that evolutionary control is possible even when gene drive cells are less fit relative to native resistant populations. This is because, even with poor gene delivery of around 1%, the gene drive population is expected to be orders of magnitude more abundant than resistant subclones at the onset of treatment[2], allowing even low-fitness gene drive cells to outcompete native resistance. The evolutionary model also reveals optimal treatment regimens. In particular, simulation results highlight the benefit of some delay between the engagement of Switch 2 and the cessation of Switch 1 (Supplementary Fig. 1a,b). Sensitivity analyses reveal that these findings are robust to variation in growth kinetics, but outcomes improve for smaller detection sizes and lower mutation rates (Supplementary Fig. 1c).

In total, these modeling results explore many conceivable failure modes with physiologically plausible parameters and predict the potential for success in forward-engineering tumor populations. While standard monotherapy is predicted to fail across all physiologically relevant conditions, simulation results indicate that selection gene drive therapy is expected to extend progression-free survival in all cases (Supplementary Fig. 1b) and potentiate eradication in most conditions (Fig. 1g). Because the transient nature of the Switch 1 selection gene is sufficient for outgrowth under targeted therapy treatment, resistant subclones that spawn in the gene drive population during Switch 1 treatment are not expected to increase in abundance relative to base gene drive cells. Instead, across simulation conditions, the unmutated gene drive population comes to dominate the tumor environment. Then, Switch 2 exploits this dominance to clear both gene drive and natively resistant cells, before cross-resistance has an opportunity to emerge.

In addition to mutational points of failure, we wanted to assess the possible spatial risks of a selection gene drive system. In particular, the bystander effect of the therapeutic Switch 2 gene requires some proximity with unmodified cells in order to eliminate them. Therefore, we expect the spatial distribution of gene drive cells and the range of bystander activity to be important determinants of therapeutic success. To anticipate spatial sources of failure, we constructed a spatial agent-based model of the selection gene drive system. The model considers a mixed population of sensitive, resistant and gene drive cells. While the initial spatial distribution of resistant cells is random, gene drive cells are seeded according to a spatial dispersion parameter (Fig. 1h,i). Additionally, the distance over which the bystander effect acts is allowed to vary. The model assumes that all cells within this 'radius of effect' are sensitive to bystander killing. For the sake of computational expediency, the model also assumes all cells have equal mitotic capacity and access to resources. Example simulations for various dispersion and bystander parameters are shown in Supplementary Videos 1–4.

Model results indicate that the selection gene drive system benefits when bystander activity is diffuse (Fig. 1j). However, simulation outcomes were relatively independent of the initial spatial distribution of gene drive cells. The spatial structure of the gene drive population affected the eradication probability for a narrow set of conditions (when the bystander range is approximately two cell lengths; Supplementary Fig. 1d). Together, these results led us to favor Switch 2 genes with diffuse activities, such as those of standard GDEPT systems[30] over other proposed therapeutic transgenes that require direct contact with their neighbors[31,32]. Given the diffusion characteristics of most activated GDEPT prodrugs, a diffusible metabolite would satisfy the design criteria suggested by our agent-based model.

Inducible drug target analogs function as 'Switch 1' genes

Our theoretical compartmental and agent-based models suggest that selection gene drives are an effective approach toward achieving evolutionary control, so we designed and assembled a genetic construct guided by these theoretical results. One natural place to attempt to build a dual-switch selection drive for cancer therapy is in any molecular oncogene for which a targeted therapy is readily available and for which patients are known to be limited by drug resistance within and outside the drug target. Therefore, when designing the Switch 1 gene, we began by engineering an inducible version of a kinase drug target. Given that oncogenic kinase activity is often the result of constitutive dimerization, we reasoned that we could controllably mimic oncogenic signaling by fusing the kinase domain of a drug target to a synthetic dimerization domain.

Here, we used an FKBP12 F36V domain, which is designed to promote homodimerization in the presence of the small molecule dimerizer AP20187, which has engineered specificity for the F36V mutant over endogenous FKBP12-containing proteins[33]. This system is attractive

Fig. 2 | Modular motifs of genetic switches demonstrate inducible fitness benefits and shared fitness costs. a, Schematic of Switch 1 vEGFR$_{erl}$ design. **b**, Switch 1 activity in S1vEGFR$_{erl}$ BaF3 cells in vitro. The monmonotonic relationship between dimerizer dose and growth rate agrees with theoretical models of ligand-induced dimerization[71]. $N = 3$ technical replicates per condition; bar plots are mean ± s.e.m. **c**, Switch 1 activity in S1vEGFR$_{erl}$ BaF3 tumors in vivo. $N = 6$ tumors (3 mice) per condition; bar plots are mean ± s.e.m. **d**, Switch 1 confers inducible erlotinib resistance in S1vEGFR$_{erl}$ BaF3 cells in vitro. Erlotinib dose response in S1vEGFR$_{erl}$ BaF3s treated with (orange) or without (gray) dimerizer (abbreviated Dim). $N = 3$ technical replicates per condition. **e**, Switch 1 activity measured by western blot in *EGFR*$^+$ PC9 cells. Sensitive (wild type), resistant (EGFR L858R/T790M) and gene drive (S1vEGFR$_{erl}$) PC9 cells were treated with erlotinib and/or dimerizer. The experiment was conducted once. **f**, Schematic of Switch 2 vCyD design. **g**, Switch 2 activity in S2vCyD BaF3 cells in vitro. 5-FC dose response in *EGFR*$^+$ BaF3s expressing S2vCyD (light purple) or a control construct (wild type; blue). $N = 3$ technical replicates per condition. **h**, Switch 2 activity in S2vCyD BaF3 cells in vivo. $N = 10$ tumors (5 mice) per treatment cohort; data are presented as mean ± s.e.m. 'NS' indicates not significant, and '***' indicates $P < 0.001$. P values (0.09 for wild type (WT) +5-FC versus S2vCyD −5-FC; 0.0009 for S2vCyD −5-FC versus S2vCyD +5-FC) calculated by two-sided t-test in base R. **i**, Switch 2 bystander activity for S2vCyD BaF3 cells. In the absence of a bystander effect, the drug effect will be restricted to S2$^+$ cells in mixed populations (gray diagonal line). Observed drug effect (purple line) is higher than the null line. $N = 3$ technical replicates per mixed population; the purple line indicates mean value. **j**, Schematic of Switch 2 vCD19 design. **k**, Immune bystander activity in S2vCD19 PC9 cells (purple) co-cultured with CD19$^-$ cells (blue). $N = 3$ technical replicates; bar plots are mean ± s.e.m.

https://doi.org/10.1038/s41587-024-02271-7

because a closely related inducible dimerizer has demonstrable activity and safety in human patients[34,35]. We selected the kinase EGFR for an initial design. To generate an inducible version of EGFR, we cloned an FKBP12 F36V fusion to the juxtamembrane, kinase and C-terminal domains of *EGFR*, which are required for dimerization-induced activation of downstream signals[36]. In addition, we included an N-terminal *Src* myristylation sequence to target our synthetic EGFR protein to the cell membrane. Finally, to maintain signaling of our EGFR switch in the presence of erlotinib (and thus enable selection under drug treatment), we introduced a resistance conferring T790M mutation (Fig. 2a). We named this initial version of a Switch 1 design of an inducibly resistant drug target 'S1vEGFR$_{erl}$'.

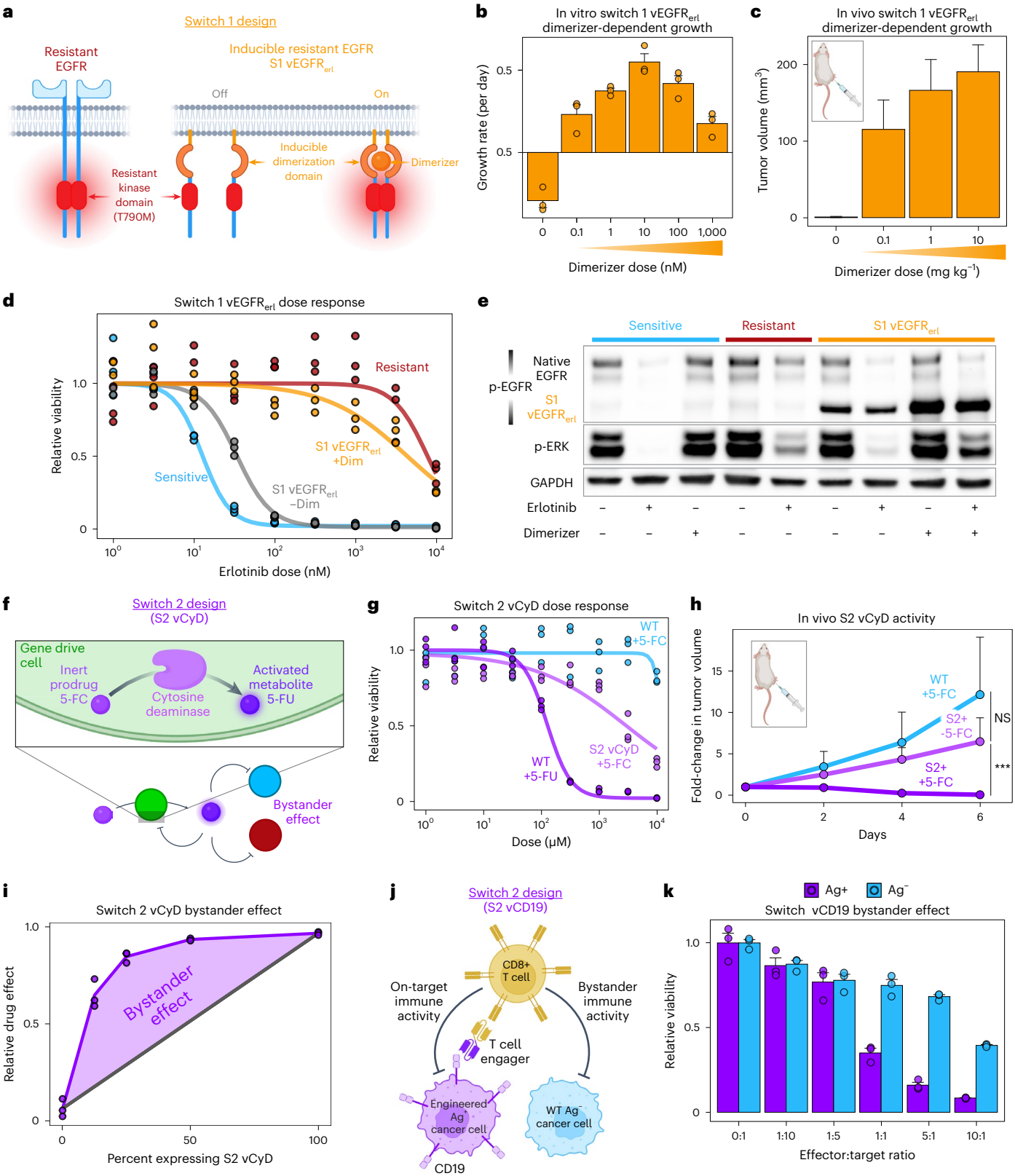

To evaluate the inducibility of S1vEGFR$_{erl}$ signaling, we expressed this synthetic gene in wild-type IL-3-dependent BaF3 cells. In the absence of IL-3, the growth of S1vEGFR$_{erl}$ BaF3 cells was found to be dimerizer dependent, suggesting that this construct can controllably mimic native kinase activity (Fig. 2b). Stimulated growth was observed across a wide range of dimerizer concentrations, indicating that kinase function is robust to the precise dose of dimerizer. To test the activity of this Switch 1 construct in vivo, we generated subcutaneous grafts of S1vEGFR$_{erl}$ BaF3 cells in mice. Once-daily administration of dimerizer stimulated tumor growth, suggesting that this system could inducibly mimic oncogenic signaling in vivo as well (Fig. 2c). Again, this activity was observed for a range of dimerizer doses, indicating that this Switch 1 gene could be robust to heterogeneity in pharmacokinetic profiles across patients[37].

To confirm the inducible resistance phenotype, we evaluated the erlotinib dose response of BaF3 cells co-transduced with S1vEGFR$_{erl}$ and the constitutively active EGFR L858R (Fig. 2d). In the absence of dimerizer, the erlotinib dose response of these cells reflected that of drug-sensitive *EGFR*$^{+}$ BaF3s. However, in the presence of dimerizer, these Switch 1 cells demonstrated erlotinib resistance. To assess the ability to induce resistance in a human *EGFR*-mutation-driven cancer cell line, we expressed S1vEGFR$_{erl}$ in the *EGFR*$^{+}$ NSCLC PC9 cells. Indeed, the Switch 1 design conferred an inducible resistance phenotype in these engineered cells (Supplementary Fig. 2a). Importantly, this inducible resistance phenotype was observed across several orders of magnitude of erlotinib concentrations.

To assess whether the synthetic S1vEGFR$_{erl}$ analog faithfully recapitulates EGFR behavior, we characterized growth pathway signaling in PC9 cells. Western blots for phospho-EGFR and phospho-ERK indicated that erlotinib blocks native EGFR autophosphorylation and MAPK activity (Fig. 2e). However, the addition of dimerizer rescues MAPK signaling in erlotinib-treated S1vEGFR$_{erl}$ PC9 cells. In total, these results suggest that S1vEGFR$_{erl}$ resembles the mechanism of native on-target resistance upon dimerizer administration.

Beyond *EGFR*, we sought to demonstrate the flexibility of the system by developing Switch 1 motifs for another therapeutically actionable kinase gene: *RET*. *RET* fusions confer sensitivity to the RET inhibitor pralsetinib in NSCLC and thyroid cancers[38]. Thus, we generated an FKBP–RET fusion protein with a pralsetinib-resistance-conferring G810R mutation[39] to develop S1vRET$_{prals}$ (Supplementary Fig. 2b). To evaluate the functionality of this orthogonal Switch 1 gene, we transduced *RET*$^{+}$ TPC1 cells with S1vRET$_{prals}$. Indeed, these engineered cells were resistant to pralsetinib in the presence of dimerizer, and sensitive otherwise (Supplementary Fig. 2c). This finding suggests that the Switch 1 dimerization motif is generalizable to other targetable kinases.

'Switch 2' motifs generate robust anticancer activity

We next considered the design of the Switch 2 gene. Guided by the results of the spatial agent-based model, we considered therapeutic genes with diffusible activity. For an initial Switch 2 construct, we evaluated cytosine deaminase (S2vCyD). Cytosine deaminase is an enzyme capable of converting the functionally inert prodrug 5-fluorocytosine (5-FC) into the potent cytotoxin 5-fluorouracil (5-FU)[30] (Fig. 2f). The CyD/5-FC system has been previously evaluated in clinical trials[40,41]. While shown to be safe, efficacy was limited by poor gene delivery—a problem that is potentially solved by leveraging potent selection. Furthermore, cytosine deaminase is an attractive Switch 2 gene because the prodrug 5-FC is an approved and well-tolerated antifungal agent[42]. The activated compound 5-FU is a well-studied chemotherapeutic with a half-century history of clinical evaluation across many cancer types[43], eliminating some of the risk associated with a completely novel chemistry.

Expressing an optimized S2vCyD[44] in BaF3 cells effectively sensitized them to 5-FC treatment (Fig. 2g). Furthermore, a panel of other human cancer lines engineered to express S2vCyD exhibited similar levels of 5-FC sensitivity, suggesting general activity across different oncogenic and biological contexts (Supplementary Fig. 2d–g). To assess the efficacy of the CyD/5-FC system in vivo, we grafted *EGFR*$^{+}$ BaF3 cells engineered to express S2vCyD in the flanks of mice. Daily dosing of 5-FC resulted in rapid tumor regression, suggesting potent in vivo activity (Fig. 2h).

To validate the bystander effect of the CyD/5-FC system, we treated mixed populations of wild-type and S2vCyD BaF3 cells with 5-FC. In the absence of a bystander effect, 5-FC/5-FU activity would be limited to S2vCyD cells. Thus, the relative drug effect would be proportional to the fraction of Switch 2 cells in a pooled population. However, 5-FC treatment in mixed cultures resulted in substantially higher killing than expected under this null hypothesis, indicating a strong bystander effect (Fig. 2i).

In addition to cytosine deaminase, we evaluated the alternative suicide gene NfsA. NfsA is an enzyme that converts the prodrug CB1954 into an activated nitrogen mustard species. An earlier version of this system has been clinically evaluated, but failed to demonstrate lasting activity, probably due to limits imposed by poor uptake of the therapeutic gene[24]. Dose response assays confirmed that 293T cells engineered to express an S2vNfsA construct were effectively sensitized to CB1954 (Supplementary Fig. 2h). In addition, assays in mixed cultures of wild-type and S2vNfsA cells confirmed a strong bystander effect in this enzyme/prodrug system as well (Supplementary Fig. 2i).

These results highlight alternative designs for the Switch 2 gene. Such alternatives may be useful, especially when targeting tumors with known recalcitrance to 5-FU treatment[45]. Furthermore, because 5-FU and nitrogen mustard agents have distinct mechanisms of action[46], there may be utility in combining these genes to achieve a combination-version of Switch 2, with nonoverlapping modes of failure[47].

Beyond the activation of a diffusible prodrug, we considered alternative Switch 2 systems with novel therapeutic potential. Previous studies have demonstrated that CD8^{+} T cells can exhibit on-tumor, off-target activity. This nonspecific cytotoxicity, mediated through FasL signaling, can kill both antigen-positive and antigen-negative cancer cells[48]. We reasoned that this activity could serve as a bystander effect in an immune version of Switch 2 (Fig. 2j). Therefore, we engineered PC9 cells to express CD19 (S2vCD19). We co-cultured these engineered cells with wild-type cells in the presence of primary T cells and the bispecific CD3/CD19 engager blinatumomab and quantified activity by flow cytometry (Supplementary Fig. 2j–l). As expected, S2vCD19 cells were targeted by the T cells (Fig. 2k). However, wild-type, antigen-negative cells were affected as well, indicating immune bystander activity in this system.

To test the alternative hypothesis that the observed effect on wild-type, antigen-negative cells was due to depletion of resources in the media caused by T cell expansion, we tested bystander activity in transwell plates. This experimental format physically separates the antigen-positive and antigen-negative cells but allows for the sharing of resources between the two populations. Results confirmed that the depletion of wild-type cells required direct contact between T cells and S2vCD19 cells (Supplementary Fig. 2m), indicating that the observed bystander effect was not an artifact of culture conditions.

These results point toward the potential to activate the immune system to generate a bystander effect in an immune version of the selection gene drive system. While CD19 was used here as an initial proof of concept, an engineered, orthogonal tumor-specific antigen could function as a Switch 2 immune target. Such a system might involve modifying cancer cells to express this antigen, selecting for the modified, antigen-positive population, and then engaging the immune system to clear both antigen-positive and antigen-negative cells. T cell tumor infiltration and migration may provide a long-distance bystander effect, satisfying the design criteria established by our spatial agent-based model (Fig. 1j). Furthermore, activation of the immune system has been shown to have an abscopal effect[49]. By encouraging

https://doi.org/10.1038/s41587-024-02271-7

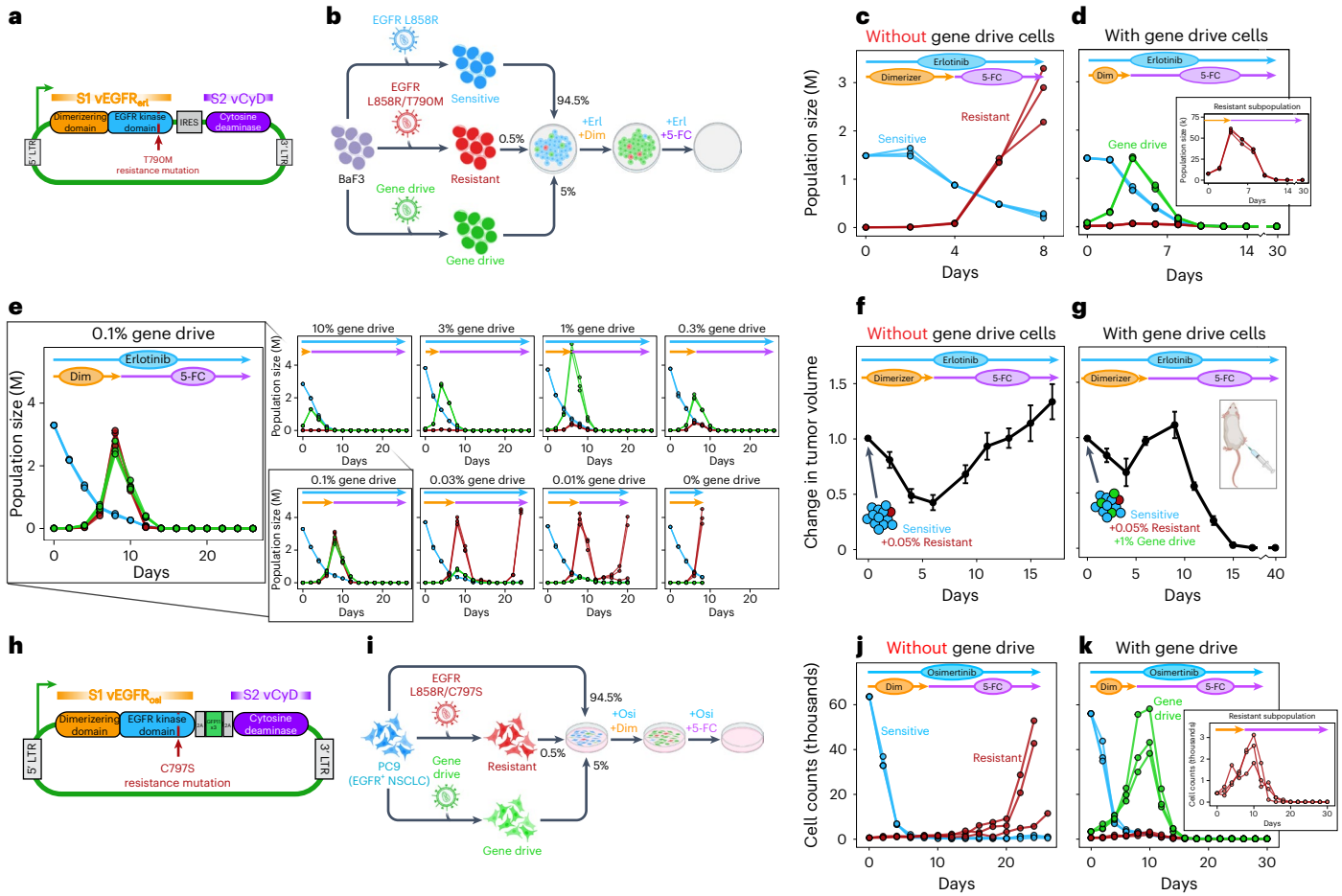

Fig. 3 | Dual-switch selection gene drives demonstrate evolutionary control. **a**, Schematic plasmid map of single lentiviral construct harboring Switch 1 (S1vEGFR$_{erl}$) and Switch 2 (S2vCyD). **b**, BaF3 cells were stably transduced with *EGFR* L858R (erlotinib-sensitive; shown in blue), *EGFR* L858R/T790M (erlotinib-resistant and mCherry$^+$; shown in red) or the dual-switch S1vEGFR$_{erl}$–S2vCyD construct (GFP$^+$; shown in green). Cells were pooled and treated with erlotinib and dimerizer. Upon outgrowth of gene drive cells, the mixed population was treated with erlotinib and 5-FC. **c**,**d**, Functionality of complete S1vEGFR$_{erl}$–S2vCyD gene drive in BaF3 cells. Sensitive (blue) and resistant (red) cells were pooled without (**c**) and with (**d**) gene drive cells (green). Blue, orange and purple arrows indicate erlotinib, dimerizer and 5-FC treatment, respectively. $N = 3$ technical replicates per condition. **e**, Functionality of complete S1vEGFR$_{erl}$–S2vCyD gene drive for various initial frequencies (0.01–10%). Resistant cells were spiked in at a constant 0.1%. Blue, orange and purple arrows indicate erlotinib, dimerizer and 5-FC treatment, respectively. $N = 3$ technical replicates per condition. **f**,**g**, Functionality of S1vEGFR$_{erl}$–S2vCyD gene drive in BaF3 tumors in vivo. Mixed populations of *EGFR*$^+$ BaF3s were prepared without (**f**) or with gene drive cells (**g**) and grafted in mice. Mice were treated once daily with erlotinib (blue arrow) and dimerizer (orange arrow) or 5-FC (purple arrow). $N = 10$ tumors (5 mice) per condition; data are presented as mean ± s.e.m. **h**, Schematic plasmid map of single lentiviral construct harboring Switch 1 (vEGFR$_{osi}$) and Switch 2 (vCyD). **i**, *EGFR*$^+$ PC9 cells (osimertinib-sensitive; shown in blue) were stably transduced with *EGFR* L858R/C797S (osimertinib-resistant and mCherry$^+$; shown in red) or the dual-switch S1vEGFR$_{osi}$–S2vCyD construct (GFP$^+$; shown in green). Cells were pooled and treated with osimertinib and dimerizer. Upon outgrowth of gene drive cells, the mixed population was treated with osimertinib and 5-FC. **j**,**k**, Functionality of complete S1vEGFR$_{osi}$–S2vCyD gene drive in PC9 cells. Sensitive (blue) and resistant (red) cells were pooled without (**j**) and with (**k**) gene drive cells (green). Blue, orange and purple arrows indicate osimertinib, dimerizer and 5-FC treatment, respectively. $N = 3$ technical replicates per condition. LTR, long terminal repeat.

interactions between immune cells and immunogenic dying cancer cells, an immune selection gene drive may enable the immune system to identify endogenous tumor neoantigens. Such activity could direct immune cells to recognize and eliminate cancer cells at distant metastatic sites that may be difficult to target with localized gene delivery.

Dual-switch gene drives demonstrate evolutionary control

Having established the activity of the Switch 1 and Switch 2 genes in isolation, we next evaluated their functionality in concert. We cloned the S1vEGFR$_{erl}$ and S2vCyD genes into a single vector (Fig. 3a) and expressed this construct in BaF3 cells that were previously transformed with activated *EGFR* to generate a complete gene drive system in an engineered model of *EGFR* dependency. To track the growth dynamics of subpopulations in mixed cultures, we engineered gene drive cells to express green fluorescent protein (GFP) and resistant cells to express mCherry. We then pooled populations of sensitive, resistant and gene drive BaF3 cells (Fig. 3b). The gene drive cells were seeded at 5% the total population, reflecting a more modest gene delivery efficiency than has been demonstrated in the clinic[24,41,50]. The resistant subpopulation was seeded at 0.5% abundance, which is orders of magnitude larger than the resistance frequency predicted by clinical measurements[2]. Thus, this population structure represented a conservative and challenging context to evaluate gene drive performance.

Monitoring of treated populations of sensitive and resistant cells by flow cytometry (Supplementary Fig. 3a–d) demonstrated that the bulk sensitive population regressed while the resistant population expanded, as expected (Fig. 3c). However, the addition of gene drive cells enabled the selection of this engineered population under dimerizer treatment, in place of the native resistant cells (Fig. 3d). Once the gene drive cells became dominant, 5-FC treatment was initiated and

https://doi.org/10.1038/s41587-024-02271-7

dimerizer was removed. The gene drive population quickly collapsed, along with the resistant population. Monitoring these cultures for 30 days revealed no outgrowth of cells, indicating complete elimination of the spiked-in resistance. Importantly, the control condition treating this same population structure with erlotinib and 5-FC at baseline (that is, Switch 2 treatment only, without an initial Switch 1 selection phase) failed to clear the resistant population, highlighting the necessity of selection under Switch 1 (Supplementary Fig. 3e). These results suggest that selection gene drive therapy can be used to clear mixed populations that would otherwise relapse under monotherapy.

Our theoretical evolutionary models suggest that the selection gene drive system could be robust to poor gene delivery, because selection in the tumor bed can compensate for inefficient tumor cell modification. To test this finding empirically, we created mixed populations of sensitive and resistant BaF3 cells (0.1% resistant population) and titered the spike-in of gene drive cells to reflect poor uptake of the genetic construct. Eradication of these mixed populations was possible for baseline gene drive frequencies as low as 0.1% (Fig. 3e). Moreover, the initial resistant subpopulation that we used here was present at 0.1% of the baseline population. This amount of pre-existing resistance is probably much more abundant than in real-world tumor populations[2]. Thus, our in vitro result suggests that selection by Switch 1 can be used to overcome remarkably low gene delivery efficiency and maximize bystander activity against competing subpopulations. Even in conditions where the resistant population eventually came to dominate (0.01–0.03% gene drive spike-in), Switch 2 bystander activity was sufficient to delay resistance outgrowth relative to the no gene drive control condition (Fig. 3e). Thus, gene drive therapy may have utility, even in cases where complete evolutionary control cannot be achieved.

Given the spatial aspects of the gene drive system, we next sought to evaluate gene drive behavior in a three-dimensional context by transplanting mixed populations of *EGFR*-transformed BaF3 cells in mice. After xenograft establishment, mice were treated daily with erlotinib and dimerizer. Upon disease progression, dimerizer was replaced with 5-FC treatment. As in the in vitro case, tumors lacking gene drive cells initially regressed and then relapsed, indicating that they had become refractory to erlotinib (Fig. 3f). Furthermore, tumors with gene drive cells that were treated with erlotinib and 5-FC at baseline (that is, no initial Switch 1 phase) exhibited similar growth dynamics, suggesting that, in the absence of selection, gene drive cells could not clear the resistant population (Supplementary Fig. 3f). Rather, the gene drive cells were probably depleted before they could generate enough bystander activity to eliminate the resistance subpopulation. However, in tumors with gene drive cells that received an initial dimerizer regimen, the 'relapsed' tumor was highly sensitive to 5-FC treatment, suggesting successful redirecting of the tumor population (Fig. 3g).

With proof of concept established in the murine BaF3 system, we next evaluated the complete gene drive system in human cancer cells. Given that frontline use of the third-generation EGFR inhibitor osimertinib has demonstrable superiority over first-generation inhibitors in the clinic[51], we decided to develop an osimertinib-compatible version of the gene drive system. Thus, we replaced the T790M erlotinib-resistance mutation with a C797S osimertinib-resistance mutation (S1vEGFR$_{osi}$). We cloned this updated Switch 1 gene and S2vCyD into a single genetic construct (S1vEGFR$_{osi}$–S2vCyD; Fig. 3h). Our design also included a split GFP system to enable the monitoring of gene drive cells in mixed populations[52]. Osimertinib dose response assays in PC9 cells transduced with the complete gene drive system confirmed the inducible resistance phenotype (Supplementary Fig. 4a). Notably, these cells retained their sensitivity to erlotinib even when Switch 1 is engaged by dimerizer treatment (Supplementary Fig. 4b). These results support the use of alternative TKIs as a fail-safe against gene drive subclones that acquire constitutive Switch 1 activity in clinical applications. PC9 cells expressing the complete gene drive construct also demonstrated sensitivity to 5-FC (Supplementary Fig. 4c) and bystander activity (Supplementary Fig. 4d).

In growth tracking experiments (Fig. 3i and Supplementary Fig. 4e–h), osimertinib treatment of pooled populations without gene drive cells ultimately selected for C797S resistance (Fig. 3j). However, in mixed cultures with a spiked-in gene drive population, we demonstrated selection for this engineered population with dimerizer treatment, followed by eradication of all cells by administering 5-FC (Fig. 3k). Here again, we observed that the Switch 1 treatment phase was required to eradicate resistance (Supplementary Fig. 4i).

Genetic 'stress tests' demonstrate system robustness

Point mutations in the drug target gene (for example, C797S) represent only one mode of treatment failure that tumor cells can exploit to evolve therapeutic resistance. In patients with NSCLC treated with frontline osimertinib, 22–39% of tumors acquire mutations or fusions in genes parallel to or downstream of EGFR[8]. Activation of these genes serves to maintain oncogenic signaling, even when EGFR kinase activity is blocked (Fig. 4a). To verify the utility of selection gene drives against these off-target alterations, we assembled a panel of oncogenes with known or suspected potential to bypass EGFR inhibition. After identifying variants that caused resistance to osimertinib in PC9 cells (Supplementary Fig. 4j), we generated mixed populations of sensitive, resistant and gene drive cells. We then treated these populations with osimertinib/dimerizer until the gene drive cells came to dominate, whereupon we initiated osimertinib/5-FC treatment. Across the panel, we observed elimination of these mixed cultures, regardless of the precise source of resistance (Fig. 4b).

Beyond arrays of spiked-in resistance, we sought to 'stress test' the selection gene drive system in more complex settings. Human cancers are defined by their remarkable genetic heterogeneity[53], but expanded in vitro populations of even millions of cells cannot effectively model the diversity of a large human tumor. To test our performance against more clinically relevant scales of tumor heterogeneity, we employed

Fig. 4 | Selection gene drives are robust to diverse forms of resistance in *cis* and in *trans*. **a**, Schematic of TKI resistance granted by activation of bypass oncogenes. Potential resistance mechanisms include mutations in alternative receptor tyrosine kinases, downstream effectors or other signaling molecules that impinge upon these downstream effectors. **b**, Functionality of complete gene drive system against various spiked-in bypass resistance populations. PC9 cells were pooled at 94.5% sensitive (wild type; blue), 5% gene drive (S1vEGFR$_{osi}$–S2vCyD; green) and 0.5% resistant (various oncogenes; red). Mixed populations were treated with osimertinib (blue arrow) and dimerizer (orange arrow) or 5-FC (purple arrow). Cells were analyzed by flow cytometry every 2 days up to 40 days. $N = 3$ technical replicates per condition. **c**, Schematic of *EGFR* single-site variant library. All codons spanning G719–H870 in the *EGFR* kinase domain (L858R background) were mutated for all possible amino acid substitutions. The final library was composed of 2,717 *EGFR* variants. **d**, Variant allele frequencies of the *EGFR* variant library. Position along the protein is shown on the *x* axis, and allele frequency is shown on the *y* axis. **e**,**f**, Functionality of gene drive system against diverse genetic library in *cis*. PC9 cells expressing the *EGFR* variant library (red) were pooled without (**e**) and with (**f**) gene drive cells (green). Blue, orange and purple arrows indicate osimertinib, dimerizer and 5-FC treatment, respectively. $N = 3$ technical replicates per condition. **g**, Schematic of genome-wide CRISPR library. The circular histogram depicts sgRNA abundance across the human genome. The final library is composed of 76,441 variants (and 1,000 nontargeting controls). **h**, Volcano plot of hits in genome-wide CRISPR osimertinib screen. More resistant knockouts are shown in red. *P* values are calculated by the MAGeCK algorithm[72] (Benjamini–Hochberg procedure). **i**,**j**, Functionality of gene drive system against diverse genetic library in *trans*. PC9 cells expressing the genome-wide CRISPR library (red) were pooled without (**i**) and with (**j**) gene drive cells (green). Blue, orange and purple arrows indicate osimertinib, dimerizer and 5-FC treatment, respectively. $N = 2$ technical replicates per condition.

https://doi.org/10.1038/s41587-024-02271-7

pooled genetic libraries to ensure oligoclonal resistance outgrowth. To assess genetic heterogeneity at the level of the drug target, we used saturating mutagenesis to generate a library of single amino acid substitutions in *EGFR* L858R (Fig. 4c). The final library was composed of 2,717 variants, spanning 94% of all possible amino acid substitutions along the EGFR kinase domain, with even representation (Fig. 4d and

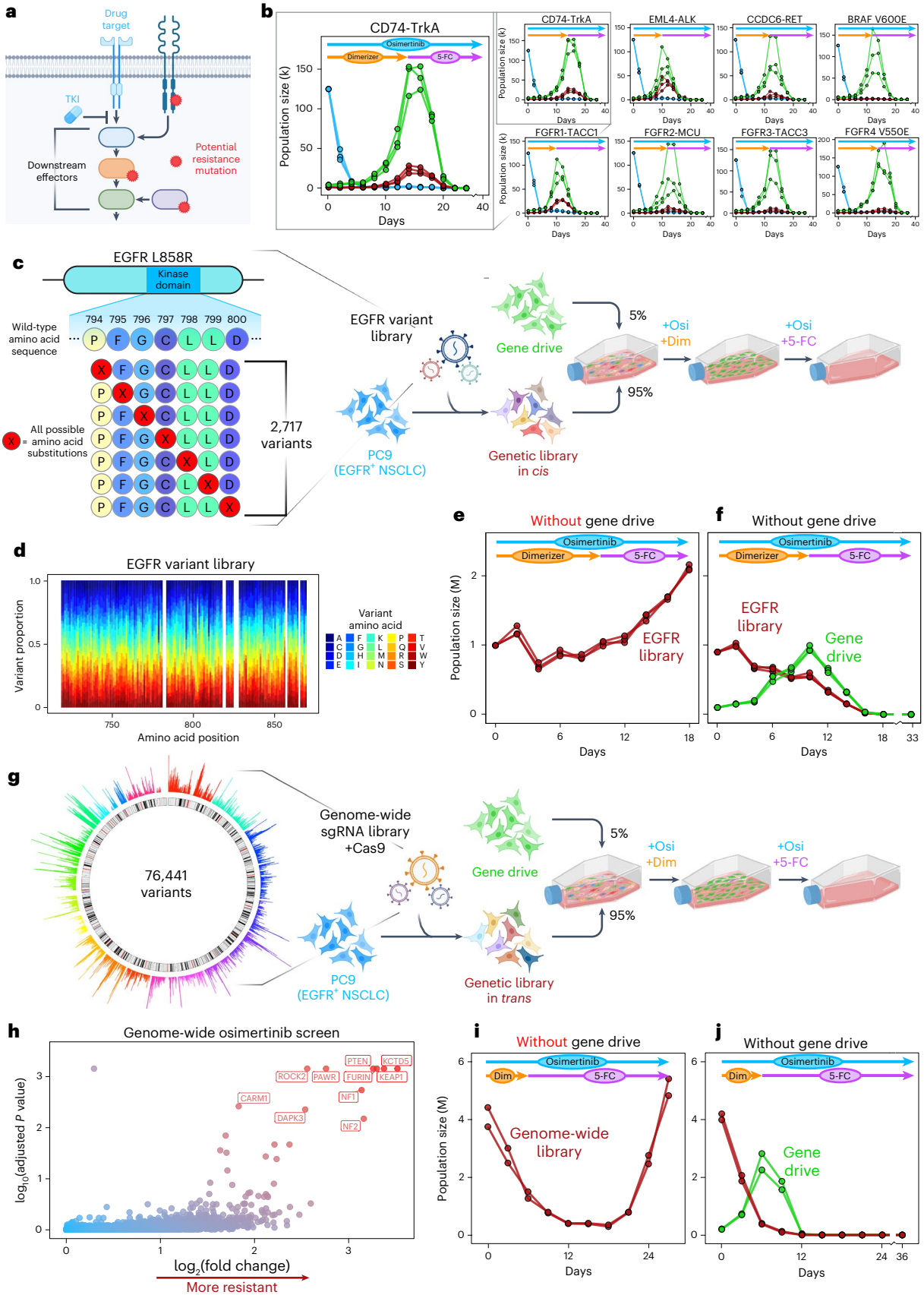

https://doi.org/10.1038/s41587-024-02271-7

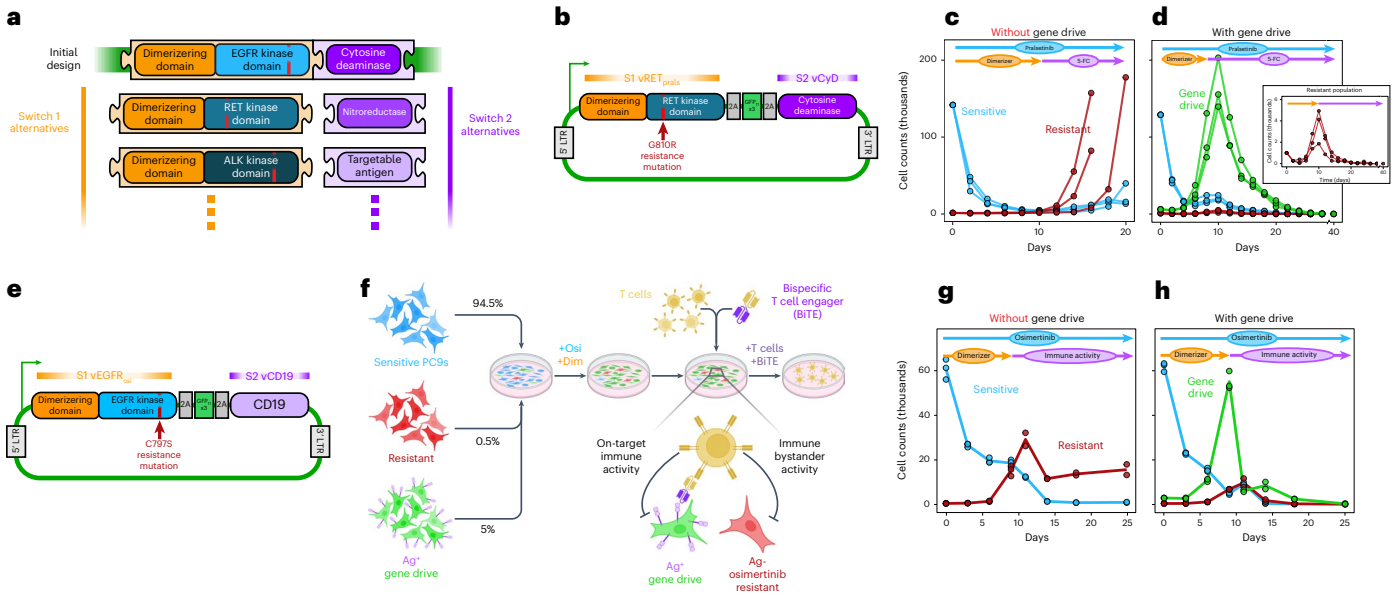

Fig. 5 | Diverse molecular designs can achieve evolutionary reprogramming. **a**, Schematic of modular dual-switch design. Alternative Switch 1 genes co-opting the kinase domains for various drug targets are shown. Additionally, orthogonal Switch 2 genes with demonstrable bystander activity are shown. **b**, Schematic plasmid map of RET gene drive construct harboring Switch 1 (vRET$_{prals}$) and Switch 2 (vCyD). **c**,**d**, Functionality of RET gene drive in *RET*$^+$ TPC1 cells. Sensitive (wild type; blue) and resistant (CCDC6-RET G810R; red) cells were pooled without (**c**) and with (**d**) gene drive cells (S1vRET$_{prals}$–S2vCyD; green). Pooled populations were treated with the RET inhibitor pralsetinib (blue arrow) and dimerizer (orange arrow) or 5-FC (purple arrow). Population dynamics for resistant cells are shown in the inset of **d**. $N = 3$ technical replicates per condition. **e**, Schematic plasmid map of immune gene drive construct harboring Switch 1 (vEGFR$_{osi}$) and Switch 2 (vCD19). **f**, Sensitive (wild type; blue), resistant (C797S and mCherry$^+$; red) and immune gene drive (S1vEGFR$_{osi}$–S2vCD19 and GFP$^+$; green) cells were pooled and treated with osimertinib and dimerizer. Upon outgrowth of the gene drive population, T cells and the CD19 bispecific T cell engager blinatumomab were added. **g**,**h**, Functionality of immune gene drive in PC9 cells. Sensitive (blue) and resistant (red) cells were pooled without (**g**) and with (**h**) gene drive cells (S1vEGFR$_{osi}$–S2vCD19; green). Blue, orange and purple arrows indicate osimertinib, dimerizer and T cells/blinatumomab, respectively. $N = 3$ technical replicates before addition of T cells/blinatumomab, and $N = 2$ technical replicates after their addition; each measurement represents a terminal time point, so no individual trajectories are presented; solid lines indicate mean value. LTR, long terminal repeat.

Supplementary Fig. 5a). Here, we expect to have a complex population of EGFR variants with a wide range of sensitivities to osimertinib. Indeed, PC9 cells transduced with this library exhibited osimertinib resistance after 12–18 days of treatment (Fig. 4e). However, we found that a small population of spiked-in gene drive cells could outcompete other variants under dimerizer treatment, and then eradicate all cells when 5-FC was administered (Fig. 4f). These results demonstrate that the selection gene drive system can be agnostic to the exact nature of on-target resistance.

In addition to mutations in the target gene and activation of bypass oncogenes, genetic alterations elsewhere in the genome can reshape more distant pathways to promote survival, even in the presence of drug[8]. To assess our gene drive system against these forms of resistance, we used a genome-wide CRISPR knockout library of 76,441 variants to create a diverse population of PC9 cells (Fig. 4g). An osimertinib screen in these cells demonstrated reproducibility and passed standard quality control metrics based on common-essential genes in the untreated conditions[54] (Supplementary Fig. 5b,c). The drug screen identified a number of resistance-conferring knockouts, including genes involved in RTK/MAPK signaling (for example, *PTEN* and *NF1/2*) and those involved in more distant pathways (for example, *KEAP1* and *KCTD5*) in agreement with previous studies[55] (Fig. 4h). We also identified potentially novel hits for osimertinib resistance, including *PAWR* and *CARM1*.

As expected, treating the CRISPR knockout PC9 population with osimertinib resulted in an initial decrease in population size, followed by the outgrowth of resistance (Fig. 4i). In spiking in gene drive cells, however, we demonstrated that Switch 1 and Switch 2 treatment could eradicate this extremely heterogeneous population (Fig. 4j). These results demonstrate the potential for a gene drive system to eliminate genetically diverse cell populations with broad sources of resistance, both within and outside the target gene. Importantly, the engineered heterogeneity used in these experiments is expected to be orders of magnitude more diverse than real-world tumors[2].

Alternative gene drive systems function in distinct contexts

The selection gene drive system was designed to be a modular platform, with the potential to 'plug and play' various Switch 1 and Switch 2 motifs (Fig. 5a). Having subjected our initial S1vEGFR$_{osi}$–s2vCyD prototype to various genetic stress tests, we set out to assess the flexibility of the system as a whole by evaluating dual-switch circuits with alternative switch motifs. To determine whether the approach is generalizable to other targets and tissues, we cloned the RET version of Switch 1 (S1vRET$_{prals}$) and S2vCyD into a single genetic construct (Fig. 5b). We expressed this system in *RET*$^+$ thyroid carcinoma TPC1 cells. In growth tracking experiments for mixed populations, we found that, in the absence of gene drive cells, pralsetinib selected for pre-existing G810R resistance (Fig. 5c). However, when a small gene drive population was spiked in, dimerizer enabled selection of these cells instead. Upon their outgrowth, 5-FC treatment eliminated both gene drive and native resistant populations (Fig. 5d). As in other contexts, gene drive populations required initial Switch 1 selection to clear pre-existing resistance (Supplementary Fig. 6a). These results suggest that the selection gene drive approach generalizes to achieve evolutionary control in different lineages and drug targets.

To develop a gene drive system with an orthogonal Switch 2 system, we cloned S1vEGFR$_{osi}$ and S2vCD19 into a single vector, generating a complete immune gene drive circuit (Fig. 5e). PC9 cells engineered to express this construct were pooled with sensitive and resistant populations and subjected to osimertinib and dimerizer.

https://doi.org/10.1038/s41587-024-02271-7

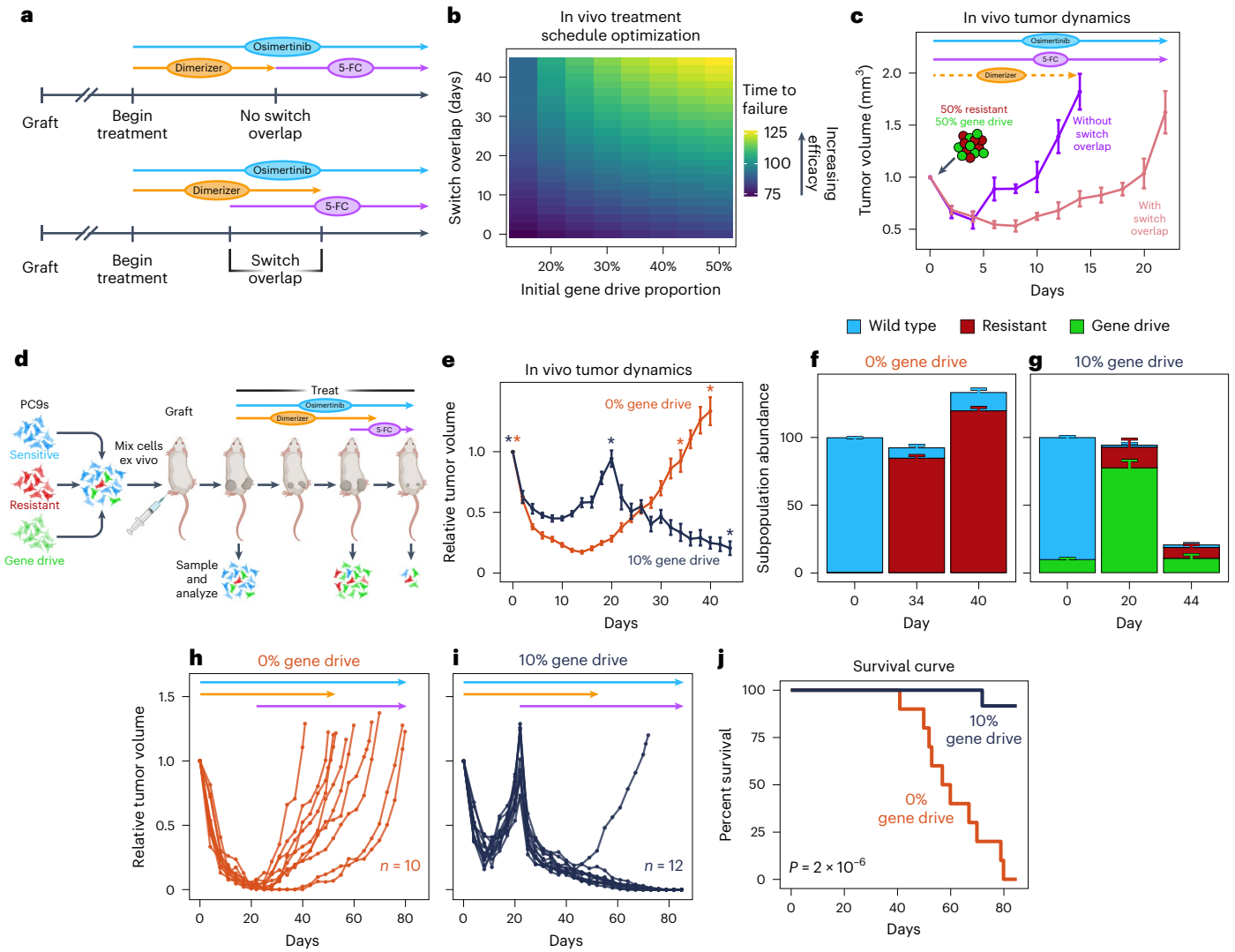

Fig. 6 | Theoretical models inform optimal treatment regimens in vivo. **a**, Theoretical treatment timelines for optimizing gene drives in vivo. **b**, Results of stochastic dynamic model for optimizing switch scheduling in vivo. See Methods for more details. **c**, Optimization of gene drive switch scheduling in PC9 tumors in vivo. Mice were grafted with mixed populations of 50% resistant and 50% gene drive cells (to emulate a possible population structure at the beginning of Switch 2 treatment) and treated once daily with osimertinib and 5-FC. Mice also received dimerizer (pink) or saline (purple) for the first 2 weeks of treatment. $N = 6$ tumors (3 mice) per condition; data are presented as mean ± s.e.m. **d**, Wild-type (blue), resistant (C797S and mCherry$^+$; red) and gene drive (S1vEGFR$_{osi}$–S2vCyD and GFP$^+$; green) PC9 cells were pooled and grafted in mice. Upon tumor establishment, mice were treated with osimertinib (blue arrow) and dimerizer (orange arrow) or 5-FC (purple arrow). At various terminal time points, subsampled tumors were collected and analyzed by flow cytometry. **e**, Functionality of schedule-optimized gene drive activity in vivo. Tumor volumes for populations of 0% gene drive (orange) and 10% gene drive (dark blue) are shown. Asterisks denote time points where subsampled tumors were analyzed by flow cytometry. $N = 6$ tumors (3 mice) per condition; data are presented as mean ± s.e.m. **f**,**g**, Subpopulation analysis of tumors undergoing gene drive therapy. Population structure for 0% gene drive (**f**) and 10% gene drive (**g**) tumors are shown. Subpopulations are scaled to tumor volumes relative to initial (D0) tumor volume. Time points correspond to asterisks in **e**. $N = 6$ tumors (3 mice) per condition and time point; data are presented as mean ± s.e.m. **h**,**i**, Long-term in vivo tumor dynamics. Volumes for tumors with 0% (**h**) or 10% (**i**) initial gene drive population. The arrows indicate period of treatment for osimertinib (blue), dimerizer (orange) and 5-FC (purple). $N = 10$ tumors (10 mice) in **h** and $N = 12$ tumors (12 mice) in **i**. **j**, Survival curve for long-term survival experiment. Significance determined by log-rank test using the 'survival' package in R[73].

Upon outgrowth, T cells and the CD19 bispecific engager blinatumomab were added to initiate anti-CD19 immune activity (Fig. 5f). Resistance emerged in mixed populations lacking gene drive cells, although their complete outgrowth may have been restricted by resource competition with T cells (Fig. 5g). However, pooled populations that included gene drive cells demonstrated sufficient selection of this engineered population to induce strong immune activity that cleared both antigen-positive gene drive cells and antigen-negative, osimertinib-resistant cells (Fig. 5h). Thus, dual-switch genetic circuits with distinct Switch 2 motifs are capable of eliminating pre-existing resistance.

Model-guided switch induction demonstrates in vivo efficacy

Having demonstrated proof of concept for diverse gene drive designs in human cancer cells in vitro, we set out to assess system functionality in vivo. We began by noting that our gene drive system exhibited moderately weaker bystander activity in human NSCLC PC9 cells (Supplementary Fig. 4d) relative to murine BaF3 cells (Fig. 2i). Indeed, evaluation of S2vCyD activity for mixed populations of PC9 cells in vivo indicated that relatively high frequencies of gene drive cells would be needed at the beginning of Switch 2 treatment to maximize potency (Supplementary Fig. 7a). Given these preliminary findings, we sought to increase efficacy by using evolutionary models to optimize switch scheduling.

We revisited the finding from our evolutionary dynamic models indicating that there exists some benefit in maintaining Switch 1 treatment for some time after initiating Switch 2 engagement, that is, switch overlap (Fig. 6a). To match the current experimental system, we reparameterized our theoretical models with growth kinetics for PC9 cells in mice. The model results predict that, given the supraphysiological resistance that we spike in our pooled populations, complete eradication of these population structures is unlikely. While we use these high-resistance populations to reproducibly stress test our approach in vivo, the theoretical model did identify regimes where switch scheduling could be optimized to prolong survival in this system. Given that a sufficiently large gene drive population is required for 5-FC activation, the model predicts a benefit in delaying the cessation of Switch 1 in order to avoid rapid clearance of gene drive cells by osimertinib. In doing so, the bystander effect of 5-FU against the osimertinib-resistant population is maximized by treating these cells as local drug factories (Fig. 6b). Eliminating these factories too rapidly means less active drug is produced locally.

To test this idea empirically, we generated mixtures of 50% gene drive and 50% resistant PC9 cells to reflect a possible population structure at the beginning of Switch 2. These pooled populations were grafted in mice. The mice were then treated with Switch 2 drugs (osimertinib and 5-FC) with or without concurrent Switch 1 engagement (dimerizer). Indeed, tumors receiving temporary dimerizer treatment exhibited a longer time to progression, suggesting a benefit to using an overlap in switch scheduling (Fig. 6c).

Next, we synthesized these findings in an in vivo pharmacodynamic experiment of dual-switch function. Pooled populations of PC9 cells were generated with gene drive frequencies ranging between 0.3% and 10%, reflecting a gene delivery efficiency that is more conservative than has been clinically demonstrated[24,41,50]. Each composition also included a 0.05% resistant population. This supraphysiological spike-in frequency was selected to ensure that resistance would be reliably detectable at the initiation of Switch 2, as a reduction in the resistant population over Switch 2 would indicate bystander activity. These mixed populations were grafted in mice and, upon tumor establishment, treated with the improved switch schedule (Fig. 6d). Tumors without gene drive subpopulations eventually became refractory to osimertinib treatment (Fig. 6e). Analysis of the tumor subpopulations confirmed that the resistant C797S population had driven relapse in these mice (Fig. 6f). However, among mice with spiked-in gene drive cells, these engineered cells came to dominate the tumor population (Fig. 6e,g). The re-engineered tumor was highly sensitized to 5-FC treatment, and subpopulation analyses indicated that the abundance of resistant cells was restricted by bystander activity (Fig. 6g). These findings were reflected in tumors with lower initial gene drive frequencies (Supplementary Fig. 7b–g).

Finally, we tested the functionality of the gene drive platform in a survival experiment. PC9 cells were mixed to generate a final composition of 3×10^{-5} resistant cells (to reflect a more clinically relevant population structure[2]) and 10% gene drive cells. Mice were subcutaneously grafted with these pooled populations and, upon tumor establishment, treated with the overlapped switch schedule. In the control arm without gene drive cells, initial regressions were invariably followed by outgrowth of osimertinib-refractory tumors (10/10 mice; Fig. 6h). In the gene drive cohort, subsets of mice were analyzed at treatment days 0 and 22 to confirm effective tumor re-engineering (Supplementary Fig. 7h), while the remaining mice were treated once daily for a total of 12 weeks. Nearly all of these mice demonstrated durable responses, with no palpable tumors at the conclusion of the study (11/12 mice; Fig. 6i). Of note, the single mouse that progressed in the gene drive group was an outlier in initial absolute tumor volume (398 cm^3 versus mean 211 cm^3; Supplementary Fig. 7i) and the smallest relative rebound tumor volume from Switch 1 engagement (Supplementary Fig. 7j). This suggests that the one-size-fits-all approach to switch scheduling could be updated in future experiments to respond to individualized tumor dynamics and maximize efficacy. Nonetheless, survival was significantly extended in the gene drive group (median survival 57 days in control arm versus not reached in gene drive arm, with no palpable tumor burden in 11 remaining mice at study conclusion, $P = 2 \times 10^{-6}$; Fig. 6j). Additionally, change in mouse weight over the course of the experiment did not significantly differ between the two cohorts (Supplementary Fig. 7k), suggesting no overt systemic toxicities associated with Switch 2 function. Together, these results support the efficacy and safety of model-guided selection gene drive therapy in vivo.

Discussion

Here, we present a conceptual framework by which evolution can be redirected to engineer tumors that are more treatable. While previous modeling studies have explored the possibility of using selection to redirect tumor evolution toward more benign states[56], and others have investigated how suicide genes can employ bystander activity against neighboring cells[57], the benefits of combining selection with bystander function were unexplored before our study. To develop this idea, we used stochastic models of evolution to propose a genetic circuit that couples an inducible fitness benefit with a shared fitness defect. We then validated this approach by employing synthetic biology techniques to develop genetic constructs compatible with existing standard-of-care therapies that could leverage evolutionary principles to eradicate heterogeneous forms of pre-existing resistance.

Our initial prototypes were built with repurposed molecular parts that can be controlled using small molecules that have already proven to be safe in humans[34,35,41,42]. Beyond these preliminary designs, we illustrated the modularity of selection gene drive motifs. Alternative Switch 1 designs demonstrated inducible fitness benefits across different drugs and tumor types. Orthogonal Switch 2 systems, including an immune-mediated anticancer mechanism, exhibited strong bystander activity. To demonstrate the evolutionary robustness of our approach, we showed that selection gene drives can eradicate astonishing levels of genetic heterogeneity within a drug target and across the genome. Finally, we employed evolutionary models to optimize the dynamics of switch engagement in vivo. All of our in vitro and in vivo experiments were performed in the presence of a large, supraphysiological population of pre-existing resistant cells. Thus, our model-driven design demonstrates the potential to establish evolutionary control over a tumor cell population otherwise destined for rapid treatment failure.

Selection gene drive technology builds upon previous advancements in the emerging field of evolutionary therapy. The practice of adaptive therapy uses evolutionary principles to inform drug dosing and/or scheduling to maintain a residual sensitive tumor cell population that suppresses the outgrowth of resistance, rather than a maximum tolerated dosing regimen that enables the competitive release of resistant subclones[58]. A recent phase II clinical study of adaptive therapy in prostate cancer reported promising results[59]. Similarly, the Switch 1 phase of selection gene drive treatment involves careful control of a population that may act to restrain resistance outgrowth, through competition for resources and space. However, gene drive therapy expands upon adaptive therapy by employing not just passive suppression of resistance variants but also active killing through Switch 2 bystander activity. Additionally, gene drive therapy does not assume a fitness cost among resistance populations[59] and can succeed in a range of parameter regimes where gene drive cells are less fit than native resistance (Fig. 1g).

Another evolution-informed therapeutic approach involves exploiting collateral sensitivities to set 'evolutionary traps'[60–62]. As in gene drive therapy, treatment strategies that leverage collateral sensitivity use sequences of drugs to guide the evolutionary trajectories toward favorable outcomes[61]. Under collateral sensitivity, administration of one drug selects for a tumor population that is sensitive to a second drug. However, natural forms of collateral sensitivity are likely

to be uncommon[63]. Rather than relying on native collateral sensitivity, gene drive therapy engineers a genetic vulnerability (Switch 2) directly into the redesigned tumor. Additionally, leveraging natural collateral sensitivity requires that tumors reliably follow an expected evolutionary trajectory. Even if tumor evolution could be predictably guided without an exogenous mechanism, it remains likely that small subclones would exist that are not subject to collateral sensitivity. Under a selection gene drive approach, Switch 1 provides a strong selection effect to reproducibly control evolution, and Switch 2 bystander activity enables the targeting of subpopulations that do not harbor the secondary genetic vulnerability directly.

There are practical considerations toward the successful translation of selection gene drives. Chief among these is delivery. In theory, tumor cells could be modified in situ to express the genetic circuit. Local delivery in nonresectable, locally advanced tumors offers a low barrier to begin translation. However, the largest impact of this technology could be achieved through systemic delivery capable of targeting distant metastases. While limiting activity to malignant cells may be challenging, there are key advantages to our system. For one, both local and systemic vector administration could make use of recent advances in the targeted delivery of nucleic acids[64–66] and tumor-specific gene expression[41,67]. Considering the low delivery requirements of gene drive therapy, our platform may be combined with these technologies to prioritize safety and selectivity (even restricting activity to a minor tumor subpopulation) over maximal delivery. Furthermore, while oncogene expression in untransformed cells generally induces senescence[68], expression of our Switch 1 oncogene analogs in tumor cells enables conditional selection. In this way, gene drive function may be intrinsically specific to malignant cells. Finally, it may be possible to leverage the ability of tumors to self-seed in order to deliver the genetic circuit to disseminated lesions in vivo[69].

Regardless of the specific delivery mechanism, by leveraging the power of selection, even the rare modification of a subset of cells is sufficient to achieve favorable outcomes. Thus, it becomes possible to prioritize a safe expression profile over a maximally efficient delivery system—a unique benefit that is not shared with other cancer gene therapy approaches. Moreover, decades of research in tumorigenesis suggest a high intrinsic barrier to transformation among normal mammalian cells, as expression of activated oncogenes without the loss of a tumor suppressor has been shown to induce senescence[70]. This differential selective effect between cancer and normal cells could provide a dramatic therapeutic window for our approach, even in the absence of targeted delivery or expression restriction. Thus, even a modest tumor selectivity for gene drive delivery and expression could exploit this tumor-specific selection to maximize safety.

In this work, we posit that tumors can be re-engineered to be more responsive to therapeutic intervention. Our initial selection gene drive designs are feasible; they behave according to quantitative models and are robust in the face of dramatic genetic and spatial failure modes. While the gene drive approach has risks, the intractability of treatment of late-stage tumors and the dramatic genetic diversity present in tumors at baseline necessitates bold new approaches. By leveraging evolutionary models, we can design tumors that reliably and effectively target their own heterogeneity.

Online content

Any methods, additional references, Nature Portfolio reporting summaries, source data, extended data, supplementary information, acknowledgements, peer review information; details of author contributions and competing interests; and statements of data and code availability are available at https://doi.org/10.1038/s41587-024-02271-7.

References

1. Navin, N. E. The first five years of single-cell cancer genomics and beyond. *Genome Res.* **25**, 1499–1507 (2015).
2. Schmitt, M. W. et al. Single-molecule sequencing reveals patterns of pre-existing drug resistance that suggest treatment strategies in Philadelphia-positive leukemias. *Clin. Cancer Res.* **24**, 5321–5334 (2018).
3. Frankell, A. M. et al. The evolution of lung cancer and impact of subclonal selection in TRACERx. *Nature* **616**, 525–533 (2023).
4. Martínez-Ruiz, C. et al. Genomic–transcriptomic evolution in lung cancer and metastasis. *Nature* **616**, 543–552 (2023).
5. Song, P. et al. Limitations and opportunities of technologies for the analysis of cell-free DNA in cancer diagnostics. *Nat. Biomed. Eng.* **6**, 232–245 (2022).
6. Short, N. J. et al. Ultra-accurate duplex sequencing for the assessment of pretreatment ABL1 kinase domain mutations in Ph^+ ALL. *Blood Cancer J.* **10**, 1–9 (2020).
7. Leighow, S. M. & Pritchard, J. R. The risks of perpetuating an evolutionary arms race in drug discovery. *Evol. Med. Public Health* **2019**, 64–65 (2019).
8. Leonetti, A. et al. Resistance mechanisms to osimertinib in EGFR-mutated non-small cell lung cancer. *Br. J. Cancer* **121**, 725–737 (2019).
9. Bozic, I. et al. Evolutionary dynamics of cancer in response to targeted combination therapy. *eLife* **2**, e00747 (2013).
10. Goldie, J. H. & Coldman, A. J. The genetic origin of drug resistance in neoplasms: implications for systemic therapy. *Cancer Res.* **44**, 3643–3653 (1984).
11. Frei, E. Curative cancer chemotherapy. *Cancer Res.* **45**, 6523–6537 (1985).
12. Palmer, A. C., Chidley, C. & Sorger, P. K. A curative combination cancer therapy achieves high fractional cell killing through low cross-resistance and drug additivity. *eLife* **8**, e50036 (2019).
13. Behan, F. M. et al. Prioritization of cancer therapeutic targets using CRISPR–Cas9 screens. *Nature* **568**, 511–516 (2019).
14. Meyers, R. M. et al. Computational correction of copy-number effect improves specificity of CRISPR–Cas9 essentiality screens in cancer cells. *Nat. Genet.* **49**, 1779–1784 (2017).
15. US Food and Drug Administration. *FDA Approves Osimertinib with Chemotherapy for EGFR-Mutated Non-small Cell Lung Cancer* (FDA, 2024).
16. Corrie, P. G. Cytotoxic chemotherapy: clinical aspects. *Medicine* **36**, 24–28 (2008).
17. Wang, Y. et al. Clinical effectiveness and clinical toxicity associated with platinum-based doublets in the first-line setting for advanced non-squamous non-small cell lung cancer in Chinese patients: a retrospective cohort study. *BMC Cancer* **14**, 940 (2014).
18. Noronha, V. et al. Gefitinib versus gefitinib plus pemetrexed and carboplatin chemotherapy in EGFR-mutated lung cancer. *J. Clin. Oncol.* **38**, 124–136 (2020).
19. Planchard, D. et al. Osimertinib with or without chemotherapy in EGFR-mutated advanced NSCLC. *N. Engl. J. Med.* **389**, 1935–1948 (2023).
20. Offin, M. et al. Tumor mutation burden and efficacy of EGFR-tyrosine kinase inhibitors in patients with EGFR-mutant lung cancers. *Clin. Cancer Res.* **25**, 1063–1069 (2019).
21. Borghaei, H. et al. Nivolumab versus docetaxel in advanced nonsquamous non-small-cell lung cancer. *N. Engl. J. Med.* **373**, 1627–1639 (2015).
22. Nasu, Y. et al. Suicide gene therapy with adenoviral delivery of HSV-tK gene for patients with local recurrence of prostate cancer after hormonal therapy. *Mol. Ther. J. Am. Soc. Gene Ther.* **15**, 834–840 (2007).
23. Topf, N., Worgall, S., Hackett, N. R. & Crystal, R. G. Regional 'pro-drug' gene therapy: intravenous administration of an adenoviral vector expressing the *E. coli* cytosine deaminase gene and systemic administration of 5-fluorocytosine suppresses growth of hepatic metastasis of colon carcinoma. *Gene Ther.* **5**, 507–513 (1998).

24. Patel, P. A phase I/II clinical trial in localized prostate cancer of an adenovirus expressing nitroreductase with CB1954 [correction of CB1984]. *Mol. Ther. J. Am. Soc. Gene Ther.* **17**, 1292–1299 (2009).
25. Rainov, N. G. A phase III clinical evaluation of herpes simplex virus type 1 thymidine kinase and ganciclovir gene therapy as an adjuvant to surgical resection and radiation in adults with previously untreated glioblastoma multiforme. *Hum. Gene Ther.* **11**, 2389–2401 (2000).
26. Sangro, B. et al. A phase I clinical trial of thymidine kinase-based gene therapy in advanced hepatocellular carcinoma. *Cancer Gene Ther.* **17**, 837–843 (2010).
27. Sagara, T. et al. Successful gene therapy requires targeting the vast majority of cancer cells. *Cancer Biol. Ther.* **21**, 946–953 (2020).
28. Windbichler, N. et al. A synthetic homing endonuclease-based gene drive system in the human malaria mosquito. *Nature* **473**, 212–215 (2011).
29. Allen, G. M. & Lim, W. A. Rethinking cancer targeting strategies in the era of smart cell therapeutics. *Nat. Rev. Cancer* **22**, 693–702 (2022).
30. Zhang, J., Kale, V. & Chen, M. Gene-directed enzyme prodrug therapy. *AAPS J.* **17**, 102–110 (2014).
31. ElOjeimy, S. et al. FasL gene therapy: a new therapeutic modality for head and neck cancer. *Cancer Gene Ther.* **13**, 739–745 (2006).
32. Touraine, R. L., Ishii-Morita, H., Ramsey, W. J. & Blaese, R. M. The bystander effect in the HSVtk/ganciclovir system and its relationship to gap junctional communication. *Gene Ther.* **5**, 1705–1711 (1998).
33. Rollins, C. T. et al. A ligand-reversible dimerization system for controlling protein–protein interactions. *Proc. Natl Acad. Sci. USA* **97**, 7096–7101 (2000).
34. Di Stasi, A. et al. Inducible apoptosis as a safety switch for adoptive cell therapy. *N. Engl. J. Med.* **365**, 1673–1683 (2011).
35. Iuliucci, J. D. et al. Intravenous safety and pharmacokinetics of a novel dimerizer drug, AP1903, in healthy volunteers. *J. Clin. Pharmacol.* **41**, 870–879 (2001).
36. Jura, N. et al. Mechanism for activation of the EGF receptor catalytic domain by the juxtamembrane segment. *Cell* **137**, 1293–1307 (2009).
37. Lin, J. H. Pharmacokinetic and pharmacodynamic variability: a daunting challenge in drug therapy. *Curr. Drug Metab.* **8**, 109–136 (2007).
38. Subbiah, V. et al. Pan-cancer efficacy of pralsetinib in patients with RET fusion-positive solid tumors from the phase 1/2 ARROW trial. *Nat. Med.* **28**, 1640–1645 (2022).
39. Subbiah, V. et al. Structural basis of acquired resistance to selpercatinib and pralsetinib mediated by non-gatekeeper RET mutations. *Ann. Oncol.* **32**, 261–268 (2021).
40. Cloughesy, T. F. et al. Durable complete responses in some recurrent high-grade glioma patients treated with Toca 511 + Toca FC. *Neuro Oncol.* **20**, 1383–1392 (2018).
41. Pandha, H. S. et al. Genetic prodrug activation therapy for breast cancer: a phase I clinical trial of erbB-2-directed suicide gene expression. *J. Clin. Oncol.* **17**, 2180–2189 (1999).
42. Vermes, A., Guchelaar, H.-J. & Dankert, J. Flucytosine: a review of its pharmacology, clinical indications, pharmacokinetics, toxicity and drug interactions. *J. Antimicrob. Chemother.* **46**, 171–179 (2000).
43. Longley, D. B., Harkin, D. P. & Johnston, P. G. 5-Fluorouracil: mechanisms of action and clinical strategies. *Nat. Rev. Cancer* **3**, 330–338 (2003).
44. Fuchita, M. et al. Bacterial cytosine deaminase mutants created by molecular engineering show improved 5-fluorocytosine-mediated cell killing in vitro and in vivo. *Cancer Res.* **69**, 4791–4799 (2009).
45. Pardini, B. et al. 5-Fluorouracil-based chemotherapy for colorectal cancer and MTHFR/MTRR genotypes. *Br. J. Clin. Pharmacol.* **72**, 162–163 (2011).
46. Gilad, Y., Gellerman, G., Lonard, D. M. & O'Malley, B. W. Drug combination in cancer treatment—from cocktails to conjugated combinations. *Cancers* **13**, 669 (2021).
47. Freytag, S. O. et al. Phase I study of replication-competent adenovirus-mediated double-suicide gene therapy in combination with conventional-dose three-dimensional conformal radiation therapy for the treatment of newly diagnosed, intermediate- to high-risk prostate cancer. *Cancer Res.* **63**, 7497–7506 (2003).
48. Upadhyay, R. et al. A critical role for fas-mediated off-target tumor killing in T cell immunotherapy. *Cancer Discov.* **11**, 599–613 (2021).
49. Janopaul-Naylor, J. R., Shen, Y., Qian, D. C. & Buchwald, Z. S. The abscopal effect: a review of pre-clinical and clinical advances. *Int. J. Mol. Sci.* **22**, 11061 (2021).
50. Roth, J. A. et al. Retrovirus-mediated wild-type P53 gene transfer to tumors of patients with lung cancer. *Nat. Med.* **2**, 985–991 (1996).
51. Soria, J.-C. et al. Osimertinib in untreated EGFR-mutated advanced non-small-cell lung cancer. *N. Engl. J. Med.* **378**, 113–125 (2018).
52. Kamiyama, D. et al. Versatile protein tagging in cells with split fluorescent protein. *Nat. Commun.* **7**, 11046 (2016).
53. Gerlinger, M. et al. Intratumor heterogeneity and branched evolution revealed by multiregion sequencing. *N. Engl. J. Med.* **366**, 883–892 (2012).
54. Dempster, J. M. et al. Extracting biological insights from the Project Achilles genome-scale CRISPR screens in cancer cell lines. Preprint at *bioRxiv* https://doi.org/10.1101/720243 (2019).
55. Zeng, H. et al. Genome-wide CRISPR screening reveals genetic modifiers of mutant EGFR dependence in human NSCLC. *eLife* **8**, e50223 (2019).
56. Maley, C. C., Reid, B. J. & Forrest, S. Cancer prevention strategies that address the evolutionary dynamics of neoplastic cells: simulating benign cell boosters and selection for chemosensitivity. *Cancer Epidemiol. Biomark. Prev.* **13**, 1375–1384 (2004).
57. Freeman, S. M. et al. The 'bystander effect': tumor regression when a fraction of the tumor mass is genetically modified. *Cancer Res.* **53**, 5274–5283 (1993).
58. Gatenby, R. A., Silva, A. S., Gillies, R. J. & Frieden, B. R. Adaptive therapy. *Cancer Res.* **69**, 4894–4903 (2009).
59. Zhang, J., Cunningham, J. J., Brown, J. S. & Gatenby, R. A. Integrating evolutionary dynamics into treatment of metastatic castrate-resistant prostate cancer. *Nat. Commun.* **8**, 1816 (2017).
60. Lin, K. H. et al. Using antagonistic pleiotropy to design a chemotherapy-induced evolutionary trap to target drug resistance in cancer. *Nat. Genet.* **52**, 408–417 (2020).
61. Zhao, B. et al. Exploiting temporal collateral sensitivity in tumor clonal evolution. *Cell* **165**, 234–246 (2016).
62. Chen, G. et al. Targeting the adaptability of heterogeneous aneuploids. *Cell* **160**, 771–784 (2015).
63. Dalin, S., Grauman-Boss, B., Lauffenburger, D. A. & Hemann, M. T. Collateral responses to classical cytotoxic chemotherapies are heterogeneous and sensitivities are sparse. *Sci. Rep.* **12**, 5453 (2022).
64. Körbelin, J. et al. Pulmonary targeting of adeno-associated viral vectors by next-generation sequencing-guided screening of random capsid displayed peptide libraries. *Mol. Ther.* **24**, 1050–1061 (2016).
65. Goertsen, D., Goeden, N., Flytzanis, N. C. & Gradinaru, V. Targeting the lung epithelium after intravenous delivery by directed evolution of underexplored sites on the AAV capsid. *Mol. Ther. Methods Clin. Dev.* **26**, 331–342 (2022).

66. Cheng, Q. et al. Selective organ targeting (SORT) nanoparticles for tissue-specific mRNA delivery and CRISPR–Cas gene editing. *Nat. Nanotechnol.* **15**, 313–320 (2020).
67. Nemunaitis, J. et al. A phase I study of telomerase-specific replication competent oncolytic adenovirus (telomelysin) for various solid tumors. *Mol. Ther. J. Am. Soc. Gene Ther.* **18**, 429–434 (2010).
68. Liu, X., Ding, J. & Meng, L. Oncogene-induced senescence: a double edged sword in cancer. *Acta Pharmacol. Sin.* **39**, 1553–1558 (2018).
69. Kim, M.-Y. et al. Tumor self-seeding by circulating cancer cells. *Cell* **139**, 1315–1326 (2009).
70. Zhu, H. et al. Oncogene-induced senescence: from biology to therapy. *Mech. Ageing Dev.* **187**, 111229 (2020).
71. Mack, E. T., Perez-Castillejos, R., Suo, Z. & Whitesides, G. M. Exact analysis of ligand-induced dimerization of monomeric receptors. *Anal. Chem.* **80**, 5550–5555 (2008).
72. Wang, B. et al. Integrative analysis of pooled CRISPR genetic screens using MAGeCKFlute. *Nat. Protoc.* **14**, 756–780 (2019).
73. Therneau, T. M. & Grambsch, P. M. *Modeling Survival Data: Extending the Cox Model* (Springer, 2000).

Methods

Description of compartmental dynamic model

See Supplementary Appendix 1 for a complete model description. In brief, the model considers a small sensitive population that expands until detection, whereupon treatment begins. A fraction of the tumor is assigned gene drive status, and then the Switch 1 treatment phase begins. Under Switch 1, gene drive cells expand. Once the tumor returns to its initial size, the Switch 2 treatment phase begins. Under Switch 2, gene drive cells produce a diffusible toxin that effects unmodified cells at a rate proportional to the fraction of gene drive cells. Over the course of tumor expansion and treatment, subclones resistant to targeted therapy or bystander killing are spawned. Additionally, gene drive cells may lose expression of the gene drive construct through mutation. The parameter ranges used were as follows: gene delivery efficiency, 0.1–32%; net growth rate, 0.005–0.02 per day; turnover rate, 1–21; tumor population at detection, 10^8–10^{11} cells; and mutation rate, 10^{-9}–10^{-6} per division. Each parameter set is simulated for 48 virtual tumors. The simulation code is available on GitHub[74].

Description of spatial agent-based model

See Supplementary Appendix 2 for a complete model description. In brief, the model considers a mixed population of sensitive, TKI-resistant and gene drive tumor cells. The initial spatial distribution of the gene drive cells is determined by a dispersion parameter, which is allowed to vary. Additionally, the distance of bystander effect (ρ) is allowed to vary. During Switch 2, cells within ρ cell lengths of a gene drive cell are subject to bystander killing. The parameter ranges used were as follows: distance of bystander effect, 0–5 cells; and dispersion of gene drive cells, 0–1. Each parameter set is simulated for 25 virtual tumors. The simulation code is available on GitHub[74].

Construct generation

PCR-based cloning was used to insert genes of interest (including *EGFR* L858R, cytosine deaminase and CD19) into the pLVX-IRES-Puro vector (Addgene). Switch 1 constructs were similarly generated by cloning target kinase domains into the pLVX-Hom-Mem1 vector (Takara). Site-directed mutagenesis was used to generate resistance variants. Proper assembly and mutation identity were confirmed by Sanger sequencing.

Cell culture

BaF3 (DSMZ), PC9 (Sigma-Aldrich), TPC1 (Sigma), HCC78 (DSMZ) and H3122 (NCI) cells were maintained in RPMI-1640 (Sigma-Aldrich) + 10% fetal bovine serum (Corning) + 1% penicillin–streptomycin (Life Technologies). Before transformation, BaF3 cells were cultured in 10 ng ml^{-1} murine IL-3 (PeproTech). Cells were grown in a 37 °C incubator with 5% CO_2.

Early-passage wild-type PC9 cells exhibited initial regression followed by rapid outgrowth in erlotinib and osimertinib, even at high concentrations, suggesting a substantial pre-existing resistance subpopulation. To develop a clean PC9 population with reproducible drug response, we isolated an EGFR inhibitor-sensitive clone. This monoclonal line served as the wild-type, sensitive population in PC9 experiments and was used to generate gene drive and resistant PC9 cells.

Lentiviral transduction

pLVX constructs were co-transfected with third-generation lentiviral packaging plasmids and VSV-G in HEK293T cells (ATCC) using calcium phosphate. The viral supernatant was collected at 48 h and used to infect the target cell. To generate fluorescently labeled BaF3 cells used in growth tracking experiments, we relied on multiple sequential rounds of infection and selection. For gene drive cells, BaF3s were infected with pLVX-Puro-IRES-GFP (Addgene), selected on puromycin, infected with pLVX-EGFR_L858R-IRES-Puro, selected on IL-3 independence, infected with pLVX-Hom-Mem1-EGFR and finally selected on erlotinib and dimerizer. For resistant cells, BaF3s were infected with Hyg-2A-mCherry (Addgene), selected on hygromycin, infected with pLVX-EGFR_L858R/T790M-IRES-Puro and selected on puromycin. Similar sequential infections and selections were used to generate fluorescently labeled resistant cells in the PC9 and TPC1 systems. To generate PC9 and TPC1 gene drive cells, cells were first infected with $GFP_{1–10}$-IRES-Puro and selected on puromycin. These cells were then infected with the appropriate gene drive construct containing a short GFP_{11} sequence. Gene drive cells were then sorted by fluorescence-activated cell sorting for reconstituted GFP.

BaF3 dimerizer-dependence assays

$S1vEGFR_{erl}$ BaF3s were seeded in 12-well plates at 100,000 per well with dimerizer (AP20187, Takara) in triplicate. Cell counts were measured on a hemocytometer every day for 4 days, and an exponential curve was fit to the data to estimate growth rates.

Engineered Switch 1 BaF3 in vivo models

All animal experiments were conducted under a protocol approved by the Institutional Animal Care and Use Committee. In the dimerizer-dependence in vivo experiment, $S1vEGFR_{erl}$ BaF3 cells were subcutaneously grafted on both flanks (3.5M per flank) of NOD-SCID mice (Jackson Labs). Mice were randomized into four cohorts (0, 0.1, 1 and 10 mg kg^{-1} dimerizer) of three mice each. Mice received 100 µl dimerizer or vehicle control (2% Tween in phosphate-buffered saline (PBS)) once daily via intraperitoneal (i.p.) injection. Tumor volumes were measured with calipers following 12 days of treatment.

Drug dose response assays

In general, all IC_{50} measurements were conducted similarly. Cells were seeded in 96-well plates at 3,000 per well triplicate, and the drug was serially diluted (10 µM to 1 nM) and added. Cell viability was measured 3 days after drug treatment using CellTiter-Glo 2.0 (Promega), and luminescence values were normalized to vehicle control conditions.

Immunoblotting

PC9 cells were seeded at 250,000 per well in 12-well plates. After 24 h, 250 nM erlotinib and/or 10 nM dimerizer was added. Four hours after drug treatment, cells were lysed on ice (LDS NuPage Buffer and Reducing Agent) and stored at −80 °C. Cell lysates were subjected to western blotting using p-EGFR (CellSignaling #2234) and p-ERK (CellSignaling #4370) primary antibodies and HRP-conjugated anti-rabbit secondary antibody (CellSignaling #7074). Primary and secondary antibodies were diluted 1:2,000 in 5% bovine serum albumin (BSA)/TBST. Signal was visualized with SuperSignal Chemiluminescent substrate reagent (ThermoFisher) on a Bio-Rad imager.

In vivo cytosine deaminase activity

Mice were randomized into three cohorts (five mice per cohort). *EGFR* BaF3 cells that did (two cohorts) or did not (one cohort) express S2vCyD were subcutaneously grafted in both flanks of the mice. Tumors were allowed to grow for 12 days, and then once-daily treatment was initiated. The wild-type cohort and one of the S2vCyD cohorts received 800 µl 500 mg kg^{-1} 5-FC via i.p. injection. The second S2vCyD cohort received 800 µl vehicle control (sterile PBS). Tumor volumes were measured every other day using calipers.

Enzyme-prodrug bystander assays (S2vCyD and S2vNfsA)

To evaluate the S2vCyD system, populations of wild-type and cytosine deaminase-expressing BaF3 cells were mixed at defined ratios and seeded at 30,000 per well in 96-well plates in triplicate, and 1 mM 5-FC was added. Cell viability was measured after 48 h using CellTiter-Glo and normalized to untreated controls. Similarly, wild-type and $S1vEGFR_{osi}$–S2vCyD PC9 cells were mixed, seeded at 20,000 per well and treated with 1 mM 5-FC.

To evaluate the S2vNfsA system, populations of wild-type and NfsA-expressing 293T cells were mixed, seeded at 20,000 per well in 96-well plates in triplicate and treated with 100 µM CB1954. Cell viability was measured after 24 h using CellTiter-Glo and normalized to untreated controls.

Immune bystander assays (S2vCD19)

Peripheral blood mononuclear cells (PBMCs) were sourced from Astarte (donor 369), and T cells were expanded using CD3/CD28 Dynabeads (ThermoFisher #11161D; 1:100 bead:cell ratio). For the immune bystander experiments, $CD19^+$ and $CD19^-$ PC9 cells were seeded 1:1 in 24-well plates at 60,000 per well. After 24 h, 1 ng ml^{-1} blinatumomab was added to all wells. At the same time, freshly thawed T cells were added at the appropriate concentration. Each target:effector ratio was conducted in triplicate. After 48 h, the supernatant and resuspended adherent cells were pooled and analyzed according to the following staining protocol. Cells were spun down (750*g* for 3 min) and resuspended in 50 µl Fc block buffer (BD Pharmingen #564220). After a 10-min incubation, 100 µl antibody mixture (1:1,000 dilution in PBS + 1% BSA) of anti-CD3/FITC (BioLegend #317301) and anti-CD19/APC (eBioscience #17-0199-42) was added. The cell suspension was incubated at 4 C for 20 minutes. After three washes in PBS + BSA, the cell suspension was analyzed by flow cytometry (BD Accuri C6 Plus).

In the transwell version of the experiment, CD19+ and $CD19^-$ cells (30,000 per well each) were seeded either together in the bottom of a transwell plate or separated with $CD19^-$ cells in the bottom well. After 24 h, 1 ng ml^{-1} blinatumomab was added to each well, in addition to 120,000 T cells (2:1 effector:target ratio). Each condition was run in triplicate. After 48 h, cell suspensions were recovered and analyzed as above.

Gene drive growth tracking in vitro

Populations of sensitive, $mCherry^+$ resistant and GFP^+ gene drive cells were mixed together. Except where otherwise noted, mixed populations consisted of 0.5% resistant cells and 5% gene drive cells. Cells were seeded in 24-well plates (1.5M per well for BaF3s and 50,000 per well for adherent cells) in triplicate, with the exception of the gene-drive titer experiment where 3M per well BaF3s were seeded in six-well plates to maintain sufficient cell numbers for low spike-in conditions. For Switch 1 conditions, 10 nM dimerizer and 250 nM erlotinib, 50 nM osimertinib or 1 µM pralsetinib were used. For Switch 2 conditions, 500 µM 5-FC replaced dimerizer in the above formulations.

Cell counts were measured every other day. For counts of adherent cells, wells were washed with PBS, trypsinized and then resuspended in RPMI. Cell suspensions were transferred to microcentrifuge tubes and vortexed, and a small aliquot (6%) was analyzed by flow cytometry (BD Accuri) to get subpopulation cell counts. The remaining cells were spun down (1,000*g* for 5 min), the supernatant was aspirated, and the cell pellet was resuspended in fresh RPMI and seeded onto a new plate. Fresh drug was added immediately. In general, Switch 2 treatment began when the gene drive population exceeded 60% of the day 0 cell counts. Cells were monitored for 2–3 weeks after apparent eradication to ensure that no remaining cells grew back.

Mouse experiments. All animal studies were approved by the Pennsylvania State University's Institutional Animal Care and Use Committee. Mice were housed at ambient room temperature in a humidity-controlled animal facility. Mice had free access to food and water. Mice were maintained on a 12:12 h light:dark cycle.

Gene drive BaF3 cells in vivo

Sensitive (*EGFR* L858R), resistant (*EGFR* L858R/T790M) and gene drive ($S1vEGFR_{erl}$–S2vCyD with EGFR L858R background) BaF3 cells were mixed ex vivo at frequencies of 98.95%, 0.05% and 1%, respectively. Mice were randomized into three cohorts (five mice per cohort): without gene drive cells; with gene drive cells but without Switch 1 treatment phase; and with gene drive cells and with Switch 1 treatment phase. Mixed populations of BaF3s were subcutaneously grafted in both flanks of mice (3M per flank). Tumors were allowed to grow for 10 days, and then once-daily treatment was initiated. During the Switch 1 phase of treatment, mice were dosed with 25 mg kg^{-1} erlotinib (prepared in 10:90 NMP:PEG400 v/v; administered via oral gavage) and 1 mg kg^{-1} dimerizer (prepared in 2% Tween in PBS, administered via i.p. injection). During the Switch 2 phase of treatment, mice were dosed with 25 mg kg^{-1} erlotinib (oral gavage) and 500 mg kg^{-1} 5-FC (i.p. injection). Tumor volumes were measured every other day.

EGFR variant library

The *EGFR* single-site variant library was synthesized and cloned by Twist Bioscience. In brief, saturating mutagenesis was used to introduce all possible amino acid substitutions (optimized for *H. sapiens* codon bias) between L718 and H870 residues (with the exception of R858) in the *EGFR* L858R kinase domain. Large-scale bacterial transformation maintained >2,000-fold library coverage. Lentivirus was prepared as above and stored at −80 °C. A test infection in PC9s with polybrene (4 µg ml^{-1}) was used to estimate the viral titer. The large-scale infection of PC9s maintained 450-fold post-selection library coverage, with a 5% infection efficiency to ensure low multiplicity of infection. A total of 1M cells (330-fold library coverage) were seeded in six-well plates in triplicate. In the gene drive conditions, gene drive cells were spiked in at 10% abundance. Switch 1 and Switch 2 formulations were prepared as previously. Cell counts were measured every other day by flow cytometry, and fresh drug was prepared for each time point.

Genome-wide osimertinib screen

The genome-wide Brunello CRISPR knockout library was ordered from Addgene. Lentivirus was prepared as above and stored at −80 °C, and a small-scale infection was used to assess infection efficiency in PC9s. PC9 cells were infected in two large-scale replicates at 200-fold post-selection library coverage, with a 5–10% infection efficiency.

For the osimertinib drug screen, the two infection replicates were divided into osimertinib and untreated populations. Each condition was seeded at 300M cells (390-fold library coverage) and treated with either 10 nM osimertinib or the equivalent volume of dimethyl sulfoxide. Cells were subcultured every 3 days to maintain high library coverage (>250-fold). After 15 days, cell pellets were collected and frozen.

Genomic DNA was extracted from cell pellets using the Qiagen Maxi Kit. Single guide RNAs (sgRNAs) were amplified using Illumina PCR primers[75] and sequenced on a HiSeq 3000. Guide counts were quantified using the Broad Institute GPP's PoolQ pipeline, with the default settings. Osimertinib enrichment/depletion was determined by count log-fold changes and adjusted *P* values, as calculated by the MAGeCK algorithm[72]. Sequencing files are available on SRA (PRJNA1081395), and analysis code is available on GitHub[74].

For the pooled CRISPR knockout gene drive experiments, fresh PC9 cells were infected with the Brunello library in duplicate at 150-fold coverage. After selection, the two infection replicates were seeded in 10 cm dishes at 4M cells per plate (50-fold coverage). In the gene drive conditions, gene drive cells were spiked in at 5% frequency. Switch 1 and Switch 2 formulations were prepared as in other growth tracking experiments. Cell counts were measured every 3 days by flow cytometry, and fresh drug was added at each time point.

$S1vEGFR_{osi}$–S2vCD19 gene drive growth tracking in vitro

Mixed populations of wild-type, $mCherry^+$ C797S (0.5%) and GFP^+ $S1vEGFR_{osi}$–S2vCD19 gene drive (5%) PC9 cells were seeded in 96-well plates at 35,000 per well. Drugs were added after 24 h to allow cells to adhere to the plate. During the Switch 1 phase, 10 nM dimerizer and 50 nM osimertinib were added to each well, and the media and drugs were replaced fresh every 3 days. At the beginning of Switch 2 (day 9 of treatment), the

medium of each well was replaced with fresh medium containing T cells and 1 ng ml^{-1} blinatumomab. T cells were added at 320,000 per well, for an approximate effector:target ratio of 5. In contrast to the S2vCyD gene drive tracking experiments, cells were not reseeded every day. Instead, enough wells were seeded at the beginning of the experiment such that at each time point a new well would be analyzed and then discarded. This was done to maintain proximity between T cells and adherent CD19$^{+/-}$ PC9 cells, as our transwell bystander experiments indicated the importance of direct interaction for bystander function. Wells were processed in triplicate by washing with PBS, trypsinizing and resuspending in RPMI and analyzed by flow cytometry.

Gene drive PC9 in vivo Switch 2 optimization experiments

To evaluate the effect of population structure on Switch 2 efficacy, resistant (*EGFR* L858R/C797S) and gene drive (S1vEGFR$_{osi}$–S2vCyD) PC9 cells were mixed ex vivo at different compositions. Final mixed populations were either 0%, 50%, 80%, 95% or 100% gene drive cells. Mice were randomized into five cohorts (three mice per cohort) and subcutaneously grafted with the appropriate cell mixture on both flanks (5M cells per flank). After tumor establishment (18 days), mice received once-daily dosing of osimertinib (prepared in 10:90 NMP:PEG400 v/v; administered via oral gavage) and 5-FC (500 mg kg^{-1} 5-FC prepared in PBS; administered via i.p. injection). Tumor volumes were measured every other day.

To evaluate the benefit of an overlap in switch scheduling, 50% resistant (*EGFR* L858R/C797S) and 50% gene drive (S1vEGFR$_{osi}$–S2vCyD) PC9 cells were mixed ex vivo to reflect a possible population structure at the beginning of Switch 2 treatment. These mixed populations were subcutaneously grafted in both flanks of six mice (5M cells per flank). After tumor establishment (18 days), mice were assigned to one of two treatment cohorts (three mice per cohort) to ensure roughly even initial tumor volumes. One cohort received only Switch 2 treatment (25 mg kg^{-1} osimertinib and 500 mg kg^{-1} 5-FC, daily), while the other received Switch 1 'overlap' treatment (25 mg kg^{-1} osimertinib, 500 mg kg^{-1} 5-FC and 1 mg kg^{-1} dimerizer, daily) for 2 weeks followed by Switch 2 treatment alone. Tumor volumes were measured every other day.

Gene drive PC9 in vivo dual-switch pharmacodynamics experiment

Wild-type, resistant (*EGFR* L858R/C797S; mCherry^{+}) and gene drive (S1vEGFR$_{osi}$–S2vCyD; GFP^{+}) PC9 cells were mixed ex vivo at different compositions. All mixtures included a constant 0.05% resistant population, but gene drive cell frequency was either 0%, 0.3%, 1%, 3% or 10%. Mice were randomized into five cohorts (nine mice per cohort) and subcutaneously grafted with the appropriate cell mixture on both flanks (5M cells per flank). Tumors were allowed to grow for 16 days, and then once-daily treatment was initiated. During the Switch 1 phase of treatment, mice were dosed with 25 mg kg^{-1} osimertinib (oral gavage) and 1 mg kg^{-1} dimerizer (i.p. injection). During the Switch 2 phase of treatment, mice were dosed with 25 mg kg^{-1} osimertinib (oral gavage) and 500 mg kg^{-1} 5-FC (i.p. injection). Treatment scheduling included a 2-week switch overlap, where mice received osimertinib, dimerizer and 5-FC. Tumor volumes were measured every other day.

Additionally, tumor subpopulations were analyzed by periodically killing mice, collecting their tumors and analyzing them by flow cytometry. For each of these time points, three mice were selected with an algorithm designed to maintain the statistical features of the population. In brief, for every possible combination of three mice, the mean and standard deviation of tumor volumes were calculated. The optimal combination was the one that minimized the difference in mean and standard deviation between sampled and unsampled mice. These time points were as follows: day 0 (the first day of Switch 1 treatment); the first day of Switch 2 treatment (when the mean tumor volume exceeded to 90% of the initial volume); and the last day of treatment (when the mean tumor volume exceeded 120% of the initial volume, or 44 days after treatment initiation, whichever came first). Tumors were enzymatically digested[76] and analyzed as single-cell suspensions by flow cytometry using the fluorescent labels of each population.

Gene drive PC9 in vivo long-term survival experiment

Mixed populations of PC9 cells were prepared ex vivo, similarly to the pharmacodynamics experiment. Here, all mixtures included a 3×10^{-5} resistant population and either 0% or 10% gene drive cells. Mice were randomized into two cohorts (10 in the control arm and 18 in the gene drive arm) and subcutaneously grafted with the appropriate cell mixture on a single flank (5M cells per flank). Tumors were allowed to grow for 16 days, and then once-daily treatment was initiated. Drug dosing was identical to the pharmacodynamics study, but a 4-week switch overlap was employed to maximize efficacy. Tumor volumes were measured every 3 days.

Additionally, tumor subpopulations in the gene drive cohort were at the beginning of Switch 1 (day 0) and Switch 2 (day 22) to confirm gene drive selection. As in the pharmacodynamics experiment, three mice were selected at each time point to minimize the difference in mean and standard deviation between selected and unselected mice. Tumors were enzymatically digested[76] and analyzed by flow cytometry.

Reporting summary

Further information on research design is available in the Nature Portfolio Reporting Summary linked to this article.

Data availability

Sequencing data associated with this work are publicly available on the NIH NCBI SRA (BioProject PRJNA1081395)[77]. All other data are available in the main text, in Supplementary Information, or on GitHub in the associated figure directory at https://github.com/pritchardlabatpsu/SelectionGeneDrives[74]. Source data are provided with this paper.

Code availability

All code associated with this work is publicly available on GitHub (https://github.com/pritchardlabatpsu/SelectionGeneDrives)[74].

References

74. pritchardlabatpsu/SelectionGeneDrives: Selection Gene Drive Code Release v1.0. *GitHub* https://doi.org/10.5281/zenodo.10840332 (2024).
75. Doench, J. G. et al. Optimized sgRNA design to maximize activity and minimize off-target effects of CRISPR–Cas9. *Nat. Biotechnol.* **34**, 184–191 (2016).
76. Rodriguez de la Fuente, L., Law, A. M. K., Gallego-Ortega, D. & Valdes-Mora, F. Tumor dissociation of highly viable cell suspensions for single-cell omic analyses in mouse models of breast cancer. *STAR Protoc.* **2**, 100841 (2021).
77. Leighow, S. M. et al. Programming tumor evolution with selection gene drives to prevent the emergence of drug resistance. Datasets. NCBI Bioproject. *NCBI* https://www.ncbi.nlm.nih.gov/bioproject/?term=PRJNA1081395 (2024).

Acknowledgements

We acknowledge L. Randolph, V. Rivera, M. Hemann and P. Bruno for their helpful comments on previous versions of the manuscript. We also thank the members of the U01 Synthetic Biology in Cancer consortium for valuable comments during the preparation of the manuscript. We also acknowledge the Huck Flow Cytometry Facility and its members, including D. R. Abrams, M. Koptchak and R. Mani. J.R.P. is supported by U01CA265709, R21EB026617, NSF RECODE CBET 2033673 and NSF Modulus MCB 2141650. This project was supported by Huck Institutes of the Life Sciences at Penn State University through the Huck Innovative and Transformational Seed Grant (HITS). Content is the responsibility of the authors and does not represent the views of the Huck Institutes.

Author contributions

S.M.L. and J.R.P. conceptualized this work. S.M.L., D.W. and J.R.P. developed the theoretical models. S.M.L., J.A.R., I.S., Z.Y. and H.I. conducted the experiments. S.Y. and M.A. provided support for in vivo studies. S.M.L. wrote the initial draft, and J.R.P. edited the manuscript. J.R.P. acquired the funds to support the project.

Competing interests

J.R.P. is a co-founder of Theseus Pharmaceuticals and holds equity in Theseus Pharmaceuticals. J.R.P. consults for and holds equity in MOMA Therapeutics. J.R.P. and S.M.L. are co-founders of Red Ace Bio. J.R.P. and S.M.L. have filed for patent protection of the work described in the manuscript.

Additional information

Supplementary information The online version contains supplementary material available at https://doi.org/10.1038/s41587-024-02271-7.

Correspondence and requests for materials should be addressed to Justin R. Pritchard.

Peer review information *Nature Biotechnology* thanks Andriy Marusyk and the other, anonymous, reviewer(s) for their contribution to the peer review of this work.

nature portfolio

Corresponding author(s): Justin Pritchard

Last updated by author(s): Apr 1, 2024

Reporting Summary

Nature Portfolio wishes to improve the reproducibility of the work that we publish. This form provides structure for consistency and transparency in reporting. For further information on Nature Portfolio policies, see our Editorial Policies and the Editorial Policy Checklist.

Statistics

For all statistical analyses, confirm that the following items are present in the figure legend, table legend, main text, or Methods section.

n/a	Confirmed
☐	☒ The exact sample size (*n*) for each experimental group/condition, given as a discrete number and unit of measurement
☐	☒ A statement on whether measurements were taken from distinct samples or whether the same sample was measured repeatedly
☐	☒ The statistical test(s) used AND whether they are one- or two-sided *Only common tests should be described solely by name; describe more complex techniques in the Methods section.*
☒	☐ A description of all covariates tested
☒	☐ A description of any assumptions or corrections, such as tests of normality and adjustment for multiple comparisons
☐	☒ A full description of the statistical parameters including central tendency (e.g. means) or other basic estimates (e.g. regression coefficient) AND variation (e.g. standard deviation) or associated estimates of uncertainty (e.g. confidence intervals)
☐	☒ For null hypothesis testing, the test statistic (e.g. *F*, *t*, *r*) with confidence intervals, effect sizes, degrees of freedom and *P* value noted *Give P values as exact values whenever suitable.*
☒	☐ For Bayesian analysis, information on the choice of priors and Markov chain Monte Carlo settings
☒	☐ For hierarchical and complex designs, identification of the appropriate level for tests and full reporting of outcomes
☐	☒ Estimates of effect sizes (e.g. Cohen's *d*, Pearson's *r*), indicating how they were calculated

Our web collection on statistics for biologists contains articles on many of the points above.

Software and code

Policy information about availability of computer code

Data collection	BD Accuri C6 Plus software was used to collect flow cytometry data. BioRad Imager (v1.1.0.04) was used to image blots.
Data analysis	Guide counts in the CRISPR screen were quantified using the Broad Institute GPP's PoolQ pipeline. Gene-level enrichment and depletion were quantified by the MAGeCK algorithm. All original data used in this study to analyze data has been deposited at https://github.com/pritchardlabatpsu/SelectionGeneDrives

For manuscripts utilizing custom algorithms or software that are central to the research but not yet described in published literature, software must be made available to editors and reviewers. We strongly encourage code deposition in a community repository (e.g. GitHub). See the Nature Portfolio guidelines for submitting code & software for further information.

Data

Policy information about availability of data

All manuscripts must include a data availability statement. This statement should provide the following information, where applicable:

- Accession codes, unique identifiers, or web links for publicly available datasets
- A description of any restrictions on data availability
- For clinical datasets or third party data, please ensure that the statement adheres to our policy

All sequencing data has been deposited in the SRA database (PRJNA1081395).All other raw data has been deposited at https://github.com/pritchardlabatpsu/SelectionGeneDrives

Research involving human participants, their data, or biological material

Policy information about studies with human participants or human data. See also policy information about sex, gender (identity/presentation), and sexual orientation and race, ethnicity and racism.

Reporting on sex and gender	N/A
Reporting on race, ethnicity, or other socially relevant groupings	N/A
Population characteristics	N/A
Recruitment	N/A
Ethics oversight	N/A

Note that full information on the approval of the study protocol must also be provided in the manuscript.

Field-specific reporting

Please select the one below that is the best fit for your research. If you are not sure, read the appropriate sections before making your selection.

☒ Life sciences ☐ Behavioural & social sciences ☐ Ecological, evolutionary & environmental sciences

For a reference copy of the document with all sections, see nature.com/documents/nr-reporting-summary-flat.pdf

Life sciences study design

All studies must disclose on these points even when the disclosure is negative.

Sample size	Sample sizes for in vitro (n=3) and in vivo experiments (n=6-12 tumors) were chosen based on results of mathematical models of predicted tumor dynamics parameterized on pilot studies to estimate effect size. Sample size for the osimertinib CRISPR screen (n=2) was selected based on standard practice for large-scale genetic screens (e.g. Doench et al. Nat Biotechnol "Optimized sgRNA design.." 2016).
Data exclusions	No data excluded.
Replication	For all in vitro evolutionary experiments, three technical relicates were performed. For in vivo evolutionary experiments, 6-12 mice were used per condition. All attempts at replication were successful.
Randomization	In general, mice were randomized prior to engraftment because different cohorts were grafted with different population structures. In cases where tumors were harvested at interim time points, mice were selected to preserve the mean and distribution of tumor volumes within the group, as described in the methods. No other experiments involved formal randomization.
Blinding	For in vitro and in vivo studies, blinding was not performed because a single researcher formulated and administered drugs, as well as took measurements.

Reporting for specific materials, systems and methods

We require information from authors about some types of materials, experimental systems and methods used in many studies. Here, indicate whether each material, system or method listed is relevant to your study. If you are not sure if a list item applies to your research, read the appropriate section before selecting a response.

Materials & experimental systems

n/a	Involved in the study
☐	☒ Antibodies
☐	☒ Eukaryotic cell lines
☒	☐ Palaeontology and archaeology
☐	☒ Animals and other organisms
☒	☐ Clinical data
☒	☐ Dual use research of concern
☒	☐ Plants

Methods

n/a	Involved in the study
☒	☐ ChIP-seq
☐	☒ Flow cytometry
☒	☐ MRI-based neuroimaging

Antibodies

Antibodies used	anti-CD3 (FITC): BioLegend #317301 (OKT3) anti-CD19 (APC): eBioscience #17-0199-42 (HIB19) anti-p-EGFR (p-Tyr1068): CellSignaling #2234 anti-p-ERK (Thr202/Tyr204): CellSignaling #4370 anti-rabbit secondary: CellSignaling #7074
Validation	CellSignaling provides validation western blots for the p-EGFR and p-ERK antibodies on their website (https://www.cellsignal.com/products/primary-antibodies/phospho-egf-receptor-tyr1068-antibody/2234 and https://www.cellsignal.com/products/primary-antibodies/phospho-p44-42-mapk-erk1-2-thr202-tyr204-d13-14-4e-xp-rabbit-mab/4370). Manufacturers of the antibodies used in flow cytometry (CD3 and CD19) provide validation flow cytometry plots on their websites (https://www.biolegend.com/nl-be/products/purified-anti-human-cd3-antibody-3642 and https://www.thermofisher.com/antibody/product/CD19-Antibody-clone-HIB19-Monoclonal/17-0199-42). Additionally, antigen-negative and antigen-overexpressed controls were used to verify specificity.

Eukaryotic cell lines

Policy information about cell lines and Sex and Gender in Research

Cell line source(s)	293T cells were purchased from ATCC (CRL-3216). PC9 cells were purchased from Millipore-Sigma (90071810). An EGFRi-sensitive PC9 clone was isolated to ensure homogeneous response to TKI in untransduced (wild-type) cells. TPC1 cells were purchased from Millipore-Sigma (SCC147). HCC78 cells were purchased from DSMZ (ACC 563). H3122 cells were sourced from the NCI (https://dtp.cancer.gov/repositories/). T-cells were expanded from PBMCs sourced from Astarte Bio (donor 369).
Authentication	Commercially validated cell lines were obtained from ATCC and Millipore Sigma. Cell lines grew and performed as expected. Morphology of each cell line was assessed by microscopy.
Mycoplasma contamination	The absence of mycoplasma contamination was confirmed by regular testing.
Commonly misidentified lines (See ICLAC register)	PC9 cells were previously known as PC14 cells. See statement from Riken BioResource Research center (original cell bank for PC9/PC14 cells: https://cell.brc.riken.jp/en/rcb/rcb0446_announce)

Animals and other research organisms

Policy information about studies involving animals; ARRIVE guidelines recommended for reporting animal research, and Sex and Gender in Research

Laboratory animals	All mice used in this study were female NOD.Cg-Prkdcscid Il2rgtm1Wjl/SzJ (#005557) mice from Jackson Laboratory. Cells were grafted when mice were between six and seven weeks of age.
Wild animals	No wild animals were used in this study.
Reporting on sex	The applicability of the findings are not sex-specific.
Field-collected samples	No field-collected samples were used in this study.
Ethics oversight	All procedures were approved by the Penn State Institutional Animal Care and Use Committee.

Note that full information on the approval of the study protocol must also be provided in the manuscript.

Plants

Seed stocks	N/A
Novel plant genotypes	N/A
Authentication	N/A

Flow Cytometry

Plots

Confirm that:

☒ The axis labels state the marker and fluorochrome used (e.g. CD4-FITC).

☒ The axis scales are clearly visible. Include numbers along axes only for bottom left plot of group (a 'group' is an analysis of identical markers).

☒ All plots are contour plots with outliers or pseudocolor plots.

☒ A numerical value for number of cells or percentage (with statistics) is provided.

Methodology

Sample preparation	Samples were prepared as described in the Methods.
Instrument	BD Accuri C6 Cytometer
Software	BD Accuri C6 Plus Software
Cell population abundance	To purify gene drive cells expressing the split GFP system, 250k GFP+ cells were sorted from transduced populations. Cells expressing only the G1-10 fraction (without the complementary G11 peptide) were used as negative controls. Purity was determined by flow cytometry one day post-sort, and was >97% GFP+.
Gating strategy	Viable populations were gated on FSC/SSC, and "positive" and "negative" gates were drawn using pure population controls. Specific gating strategies are shown in Supplemental Figures 2j-l, 3a-d, and 4e-h.

☒ Tick this box to confirm that a figure exemplifying the gating strategy is provided in the Supplementary Information.